Impacts of biomass burning in Southeast Asia on ozone and reactive nitrogen over the western Pacific in spring

Y. Kondo,[1] Y. Morino,[1] N. Takegawa,[1] M. Koike,[2] K. Kita,[3] Y. Miyazaki,[1] G. W. Sachse,[4] S. A. Vay,[4] M. A. Avery,[4] F. Flocke,[5] A. J. Weinheimer,[5] F. L. Eisele,[5] M. A. Zondlo,[5,6] R. J. Weber,[7] H. B. Singh,[8] G. Chen,[4] J. Crawford,[4] D. R. Blake,[9] H. E. Fuelberg,[10] A. D. Clarke,[11] R. W. Talbot,[12] S. T. Sandholm,[7] E. V. Browell,[4] D. G. Streets,[13] and B. Liley[14]

Received 2 October 2003; revised 15 March 2004; accepted 29 April 2004; published 1 July 2004.

[1] Aircraft measurements of ozone (O_3) and its precursors (reactive nitrogen, CO, nonmethane hydrocarbons) were made over the western Pacific during the Transport and Chemical Evolution Over the Pacific (TRACE-P) campaign, which was conducted during February–April 2001. Biomass burning activity was high over Southeast Asia (SEA) during this period (dry season), and convective activity over SEA frequently transported air from the boundary layer to the free troposphere, followed by eastward transport to the sampling region over the western Pacific south of 30°N. This data set allows for systematic investigations of the chemical and physical processes in the outflow from SEA. Methyl chloride (CH_3Cl) and CO are chosen as primary and secondary tracers, respectively, to gauge the degree of the impact of emissions of trace species from biomass burning. Biomass burning is found to be a major source of reactive nitrogen (NO_x, PAN, HNO_3, and nitrate) and O_3 in this region from correlations of these species with the tracers. Changes in the abundance of reactive nitrogen during upward transport are quantified from the altitude change of the slopes of the correlations of these species with CO. NO_x decreased with altitude due to its oxidation to HNO_3. On the other hand, PAN was conserved during transport from the lower to the middle troposphere, consistent with its low water solubility and chemical stability at low temperatures. Large losses of HNO_3 and nitrate, which are highly water soluble, occurred in the free troposphere, most likely due to wet removal by precipitation. This has been shown to be the major pathway of NO_y loss in the middle troposphere. Increases in the mixing ratios of O_3 and its precursors due to biomass burning in SEA are estimated using the tracers. Enhancements of CO and total reactive nitrogen (NO_y), which are directly emitted from biomass burning, were largest at 2–4 km. At this altitude the increases in NO_y and O_3 were 810 parts per trillion by volume (pptv) and 26 parts per billion by volume (ppbv) above their background values of 240 pptv and 31 ppbv, respectively. The slope of the O_3-CO correlation in biomass burning plumes was similar to those observed in fire plumes in northern Australia, Africa, and Canada. The O_3 production efficiency (OPE) derived from the O_3-CO slope and NO_x/CO emission ratio (ER) is shown to be positively correlated with the C_2H_4/NO_x ER, indicating that the C_2H_4/NO_x ER is a critical parameter in determining the OPE. Comparison of the net O_3 flux across the western Pacific region and total O_3 production due to biomass burning in

[1]Research Center for Advanced Science and Technology, University of Tokyo, Tokyo, Japan.
[2]Department of Earth and Planetary Science, Graduate School of Science, University of Tokyo, Tokyo, Japan.
[3]Department of Environmental Science, Graduate School of Science, Ibaraki University, Ibaraki, Japan.
[4]NASA Langley Research Center, Hampton, Virginia, USA.
[5]National Center for Atmospheric Research, Boulder, Colorado, USA.
[6]Southwest Sciences, Inc., Santa Fe, New Mexico, USA.
[7]Department of Earth and Atmospheric Sciences, Georgia Institute of Technology, Atlanta, Georgia, USA.
[8]NASA Ames Research Center, Moffett Field, California, USA.
[9]Department of Chemistry, University of California, Irvine, California, USA.
[10]Department of Meteorology, Florida State University, Tallahassee, Florida, USA.
[11]School of Ocean and Earth Science and Technology, University of Hawaii at Manoa, Honolulu, Hawaii, USA.
[12]Institute for the Study of Earth, Oceans, and Space, University of New Hampshire, Durham, New Hampshire, USA.
[13]Argonne National Laboratory, Argonne, Illinois, USA.
[14]National Institute of Water and Atmospheric Research, Lauder, New Zealand.

0148-0227/04/2003JD004203$09.00

SEA suggests that about 70% of O_3 produced was transported to the western Pacific. *INDEX TERMS:* 0322 Atmospheric Composition and Structure: Constituent sources and sinks; 0345 Atmospheric Composition and Structure: Pollution—urban and regional (0305); 0365 Atmospheric Composition and Structure: Troposphere—composition and chemistry; 0368 Atmospheric Composition and Structure: Troposphere—constituent transport and chemistry; *KEYWORDS:* biomass burning, ozone, NO_y

Citation: Kondo, Y., et al. (2004), Impacts of biomass burning in Southeast Asia on ozone and reactive nitrogen over the western Pacific in spring, *J. Geophys. Res.*, *109*, D15S12, doi:10.1029/2003JD004203.

1. Introduction

[2] Biomass burning is an important source of many trace gases (e.g., nitrogen oxides (NO_x), carbon dioxide (CO_2), carbon monoxide (CO), methane (CH_4), nonmethane hydrocarbons (NMHCs), oxygenated organic compounds, and methyl chloride (CH_3Cl)) [*Crutzen and Andreae*, 1990; *Andreae et al.*, 1996; *Blake et al.*, 1996; *Andreae and Marlet*, 2001; *Yokelson et al.*, 2003]. Reactions of these trace gases lead to the formation of O_3 and aerosols, which strongly influence chemical environments and radiation budgets on regional and global scales. Generally, biomass burning occurs most extensively in tropical and subtropical regions. Emissions of NO_x and CO from Africa and South America constitute a large fraction of global biomass burning emissions, and those from Southeast Asia (SEA), Indonesia, and Australia also make substantial contributions [*Galanter et al.*, 2000]. Extensive fires also occur each summer in the boreal forests in midlatitude temperate regions. Despite the relatively small average area burned, intensive boreal forest fires, which occurred in Siberia/northern China and Canada, have been observed to significantly impact regional air quality, including O_3 levels [e.g., *Phadnis and Carmichael*, 2000; *Kajii et al.*, 2002; *McKeen et al.*, 2002].

[3] The impact of biomass burning on tropospheric chemistry over Africa, South America, Indonesia, and Australia has been widely studied by ground-based and airborne measurements [e.g., *Fishman et al.*, 1996; *Harriss et al.*, 1988, 1990; *Lindesay et al.*, 1996; *Blake et al.*, 1999; *Thompson et al.*, 2001; *Kondo et al.*, 2002; *Takegawa et al.*, 2003a, 2003b]. Long-range transport of plumes impacted by biomass burning in these regions has also been studied by aircraft measurements over the South Pacific and tropical Pacific [e.g., *Hoell et al.*, 1999; *Kondo et al.*, 2002]. In contrast, studies of the effects of biomass burning in SEA on regional chemical composition are very limited. *Elvidge and Baugh* [1996] identified peninsular SEA (primarily Thailand, Myanmar, Laos, Cambodia, and Vietnam) and east-central India (Orissa Province) as the two major areas of biomass burning in SEA and India in February–March using satellite remote sensing data. Burning of forest, savanna/grassland, and crop residue are estimated to be the major sources of NO_x, CO, and NMHCs emitted by biomass burning in the five countries of SEA [*Streets et al.*, 2003b]. Increases in O_3 in plumes impacted by biomass burning over SEA in spring were detected by ozonesonde measurements over Hong Kong and aircraft sampling during the Pacific Exploratory Mission (PEM)-West B [*Chan et al.*, 2000, 2003]. Ground-based measurements of CO and O_3 in Thailand indicated effects of biomass burning on these species in the dry season [*Pochanart et al.*, 2001, 2003]. The spatial extent of the effects of biomass burning strongly depends on transport processes, especially transport from the boundary layer to the free troposphere, as well as chemical processes. Emissions of trace species from biomass burning and their chemical and transport processes need to be understood in order to assess the overall impact of biomass burning in this region on the chemical environment over the western Pacific. There have been no simultaneous measurements of key species to enable this investigation, however. In this study, we have investigated these processes and assessed the impacts of biomass burning by using chemical data obtained by aircraft measurements during the Transport and Chemical Evolution over the Pacific (TRACE-P) campaign.

2. Aircraft Data

[4] In situ chemical data obtained on board the NASA P-3B and DC-8 aircraft were used in this study, including CO, CH_3Cl, hydrogen cyanide (HCN), methyl cyanide (CH_3CN), tetrachloroethene (C_2Cl_4), NO_x, NO_y, PAN, HNO_3, aerosol nitrate (NO_3^-), aerosol size distribution, NMHCs, O_3, and H_2O. The techniques and accuracies of these measurements are summarized in Table 1. The measurements of NO_3^-, HNO_3, and NO_y are explained here because of differences in the techniques used for the measurements on board the P-3B and DC-8.

[5] Concentrations of NO_3^- in aerosol were measured on board the P-3B by the Particle into Liquid Sampler (PILS) [*Weber et al.*, 2001; *Orsini et al.*, 2003]. The particle collection efficiency of PILS was 90% for diameters smaller than 0.7 μm and decreased to 50% at 1.2 μm. The collection efficiency for diameters larger than 3 μm was close to zero. On board the DC-8, the NO_3^- concentration was measured by filter sampling, followed by ion chromatographic analysis [*Dibb et al.*, 2003].

[6] HNO_3 was measured by a chemical ionization mass spectrometer [*Zondlo et al.*, 2003] on board the P-3B and therefore represents gas-phase HNO_3. On board the DC-8, HNO_3 was collected by mist chamber, followed by ion chromatographic analysis [*Dibb et al.*, 2003]. Because HNO_3 was measured simultaneously with NO_3^- in fine particles on board the P-3B, only the P-3B HNO_3 data were used for analysis combined with submicron NO_3^-.

[7] On board the P-3B, NO_y was measured by a chemiluminescence technique combined with a gold catalytic converter heated at 300°C [*Kondo et al.*, 1997a, 2003]. The inlet was made of 3/8-inch outer diameter Teflon tubing directed rearward. Effects of particulate NO_3^- on the NO_y measurements were evaluated using simple aerodynamical calculations [*Hinds*, 1998]. Particles with Stokes numbers smaller than 0.03 (particle diameter <0.3 μm) follow streamlines of sample air because of their negligibly small

Table 1. Measurements Aboard the NASA P-3B and DC-8 Aircraft During TRACE-P

Species	Aircraft	Technique	Accuracy	1-σ Precision	Reference
CO	P-3B, DC-8	differential absorption technique using a tunable diode laser	±2%	±1%	*Sachse et al.* [1987]
Ozone	P-3B, DC-8	chemiluminescence	3% or 2 ppbv	1% or 0.5 ppbv	*Avery et al.* [2001]
NO, NO_2, NO_y	P-3B	chemiluminescence	±8% (NO), ±20% (NO_2), ±18% (NO_y)	±6 pptv at 50 pptv (NO), ±4 pptv at 70 pptv (NO_2), ±16 pptv at 500 pptv (NO_y)	*Kondo et al.* [1997a]
NO, NO_2	DC-8	Photofragmentation two-photon laser-induced fluorescence	±20–30%	±20–30%	*Bradshaw et al.* [1999]
PAN	P-3B	GC/ECD	±10%	±5%	
PAN	DC-8	GC/ECD	LOD: 1 pptv ±20%	±10%	*Singh et al.* [1996]
HNO_3	P-3B	CIMS	±15–25%	±15–25%	*Zondlo et al.* [2003]
HNO_3	DC-8	mist chamber technique	±10–20%	±10–20%	*Dibb et al.* [2003]
NO_3^-	P-3B	particle-into-liquid sampler-IC	LOD: 0.1 μg m^{-3}		*Weber et al.* [2001]
NO_3^-	DC-8	filter sampling/IC			*Dibb et al.* [2003]
NMHCs/halocarbons	P-3B, DC-8	grab sample/GC	±2–20%	±1–3%	*Blake et al.* [2003]

inertia. At Stokes numbers greater than 1 (particle diameters >3 μm), particles do not follow the streamlines that curve into the rearward facing inlet. This size cutoff is similar to that of PILS. It has been found that the concentrations of NO_3^- in fine aerosols measured by the PILS agreed well with the values of $NO_y - (NO_x + HNO_3 + PAN)$ when NO_3^- was in the form of HN_4NO_3 (Y. Miyazaki et al., manuscript in preparation, 2004). These results are consistent considering that ammonium nitrate evaporates when heated at 300°C in the NO_y gold converter. Therefore, for the present analysis, the direct NO_y measurements on board the P-3B are considered to represent gas-phase NO_y + nonrefractory NO_3^- in fine aerosols, where nonrefractory means volatile at 300°C. Because NO_y was not directly measured on board the DC-8, we defined NO_y as the sum of independently measured NO_x (NO + model calculated NO_2), PAN, and HNO_3.

3. Biomass Burning Activity in SEA

[8] Areas of active biomass burning in SEA during TRACE-P can be identified by the hot spot data from the Along Track Scanning Radiometer (ATSR-2) satellite sensor, as shown in Figure 1a. A hot spot is defined as a region where the 3.7-μm thermal channel signal exceeds 312 K determined from nighttime ATSR data. The field of view pixel size is 1 × 1 km at the center of the nadir swath (http://earth.esa.int/rootcollection/eeo4.10075). Biomass burning was most frequent at latitudes of 10°–30°N in SEA and India. The median numbers of hot spots observed at 10°–30°N and 70°–120°E in each month during 1996–2001 are shown in Figure1b. The data for 2001 are also shown in this figure. Biomass burning activity in this region generally exhibits an annual maximum in February–April [*Streets et al.*, 2003b]. Biomass burning activity in March (during the TRACE-P aircraft sampling) was somewhat lower in 2001 than the average, according to Figure 1. A more detailed comparison of biomass burning activities for 2001 versus climatological estimates was made by *Heald et al.* [2003].

[9] We used two chemical tracers to distinguish biomass burning plumes from urban pollution plumes. CH_3Cl has been used as a tracer of the combustion of biomass and biofuel, and C_2Cl_4 as an industrial tracer [*Blake et al.*, 1996, 1999]. Their relatively long lifetimes of 1.3 and 0.4 years, respectively [*Keene et al.*, 1999], allow them to be used to identify long-range transport. The concentrations of these species were quantified from whole air samples collected on both the P-3B and DC-8. Representative background values for CH_3Cl and C_2Cl_4 during TRACE-P were 550 parts per

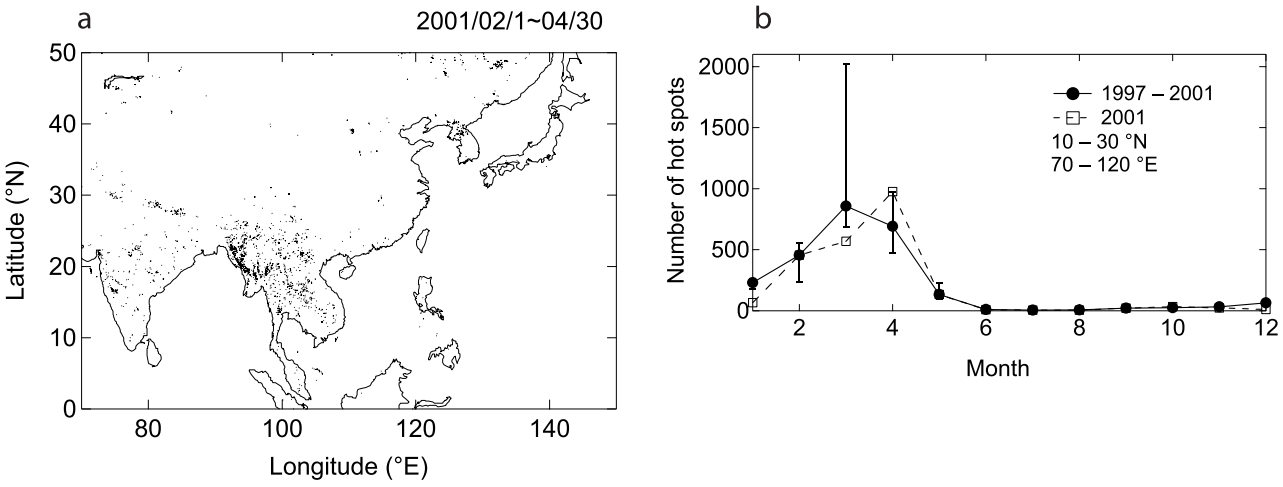

Figure 1. (a) Distribution of hot spots from 1 February to 30 April 2001 observed by the Along Track Scanning Radiometer (ATSR)-2. (b) Monthly median hot spot numbers in the region of 10°–30°N and 70°–120°E between 1997 and 2001 (solid circles). The bars indicate the central 67% values. The data for 2001 are shown as open squares.

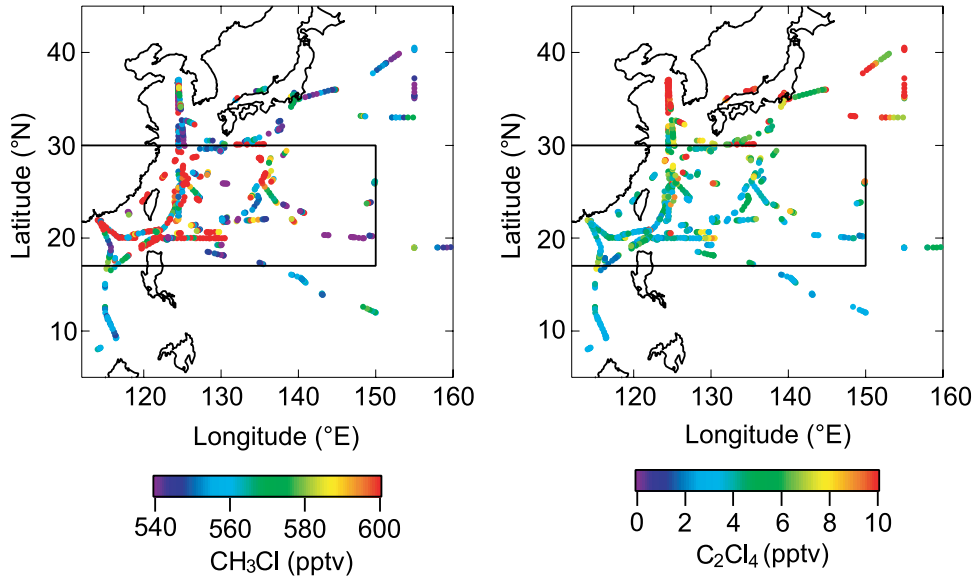

Figure 2. Horizontal distributions of CH_3Cl and C_2Cl_4 in the LT observed during the TRACE-P period. The study region is marked with rectangles.

trillion by volume (pptv) and 3 pptv, respectively. HCN and CH_3CN are also known to be emitted predominantly from biomass burning [*Andreae and Marlet*, 2001]. These species were measured only on the DC-8. Consistently, CH_3Cl was highly correlated with HCN and CH_3CN ($r^2 = 0.80$) at 2–4 km (lower troposphere; LT) in the plumes strongly impacted by biomass burning in SEA during TRACE-P (not shown), confirming that CH_3Cl is a good tracer for biomass burning. Our analyses are focused on these air masses. Inhomogeneity of sources and the oceanic sink of HCN and CH_3CN can degrade the correlations at locations distant from regions of intense biomass burning [*Singh et al.*, 2003].

[10] The horizontal distributions of these tracers in the LT over the western Pacific are shown in Figure 2. The air masses with high CH_3Cl (>600 pptv) were mostly observed at 17°–30°N, while those with high C_2Cl_4 (by up to 15 pptv) were observed mainly north of 30°N. Similar latitudinal gradients were observed at 4–8 km (middle troposphere; MT) and 0–2 km (boundary layer; BL), although they are not shown here. It should be noted, however, that even at 17°–30°N, C_2Cl_4 mixing ratios in the BL were considerably higher (by up to 20 pptv) than in the LT and MT. A majority of the BL air was transported from the north and was much more strongly impacted by emissions of C_2Cl_4 from East Asia, as discussed in section 4. These results show that in general, air masses sampled at 17°–30°N were strongly influenced by biomass burning, while those sampled north of 30°N were influenced by industrial activities. For the present study, we focus on the data obtained in the region of 17°–30°N and 110°–150°E, as marked in Figure 2, which is referred to as the study region.

4. Meteorological Conditions and Air Mass Classification

[11] The meteorological conditions during TRACE-P are described in detail by *Fuelberg et al.* [2003]. Here we highlight specific points relevant to the present analysis. The monthly mean streamlines at 850 hPa (BL), 700 hPa (LT), and 500 hPa (MT) for March 2001 were calculated using National Centers for Environmental Prediction (NCEP) reanalysis data and are shown in Figure 3. At 700 and 500 hPa, the strong northwesterlies at latitudes higher than 30°N were associated with the polar jet. Air over peninsular SEA entered the study region along the clockwise flow associated with the subtropical high-pressure system and westerlies dominating in the study region.

[12] At 850 hPa, warm air from the prevailing anticyclone centered in the central Pacific (shown in Figure 1 of *Miyazaki et al.* [2003]) moved into this region from the south, as seen in Figure 3. It converged with cold air originating from the Siberian anticyclone over SEA in March, which is the monsoon transition period from the dry to wet seasons. The instability of air associated with this convergence led to occasional convection as seen from the precipitation map shown by *Miyazaki et al.* [2003]. The convection is also seen from the cloud top height determined by the blackbody brightness temperature (T_{BB}) observed by the Geostationary Meteorological Satellite (GMS). We selected optically thick clouds by using GMS infrared (IR) data at two different wavelengths (10.5–11.5 μm and 11.5–12.5 μm). In general, convective clouds are optically thick, whereas cirrus clouds are optically thin. The T_{BB} over the peninsular SEA frequently reached 270 K (4–5 km) and occasionally 210 K (13 km). The importance of convection over SEA in spring in transporting trace species emitted by biomass burning is also discussed by *Liu et al.* [2003].

[13] The flow fields shown in Figure 3 largely determined the origins of air masses sampled in the study region. Figures 4a–4c show the 5-day back trajectories of air masses sampled in the BL, LT, and MT. These trajectories were calculated by the Florida State University (FSU) Kinematic Trajectory Model [*Fuelberg et al.*, 2003] using European Centre for Medium-Range Weather Forecasts

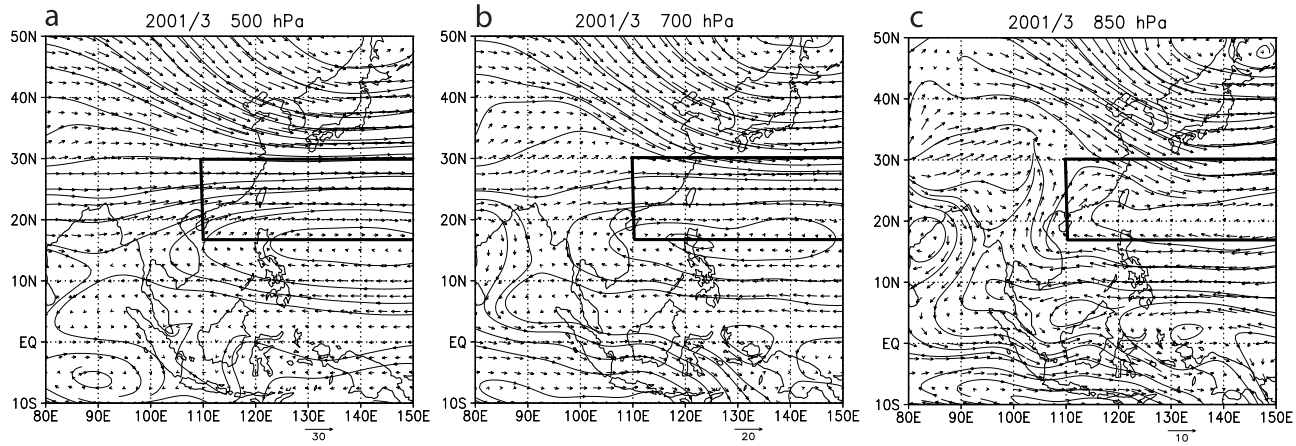

Figure 3. The mean flow patterns at (a) 500, (b) 700, and (c) 850 hPa in March 2001. Thin lines and arrows indicate streamlines and wind vectors, respectively. The study region is marked with rectangles.

(ECMWF) meteorological data on a 1.0° × 1.0° latitude-longitude grid. Sampled air masses were classified into four categories based on these trajectories. SEA air masses were defined as those passing over the intense biomass burning region south of 28°N. Northeast Asian (NEA) air masses are those transported from north of 28°N over the Asian continent to the study region at 17°–30°N. Air masses passing over the two regions (north and south of 28°N) on

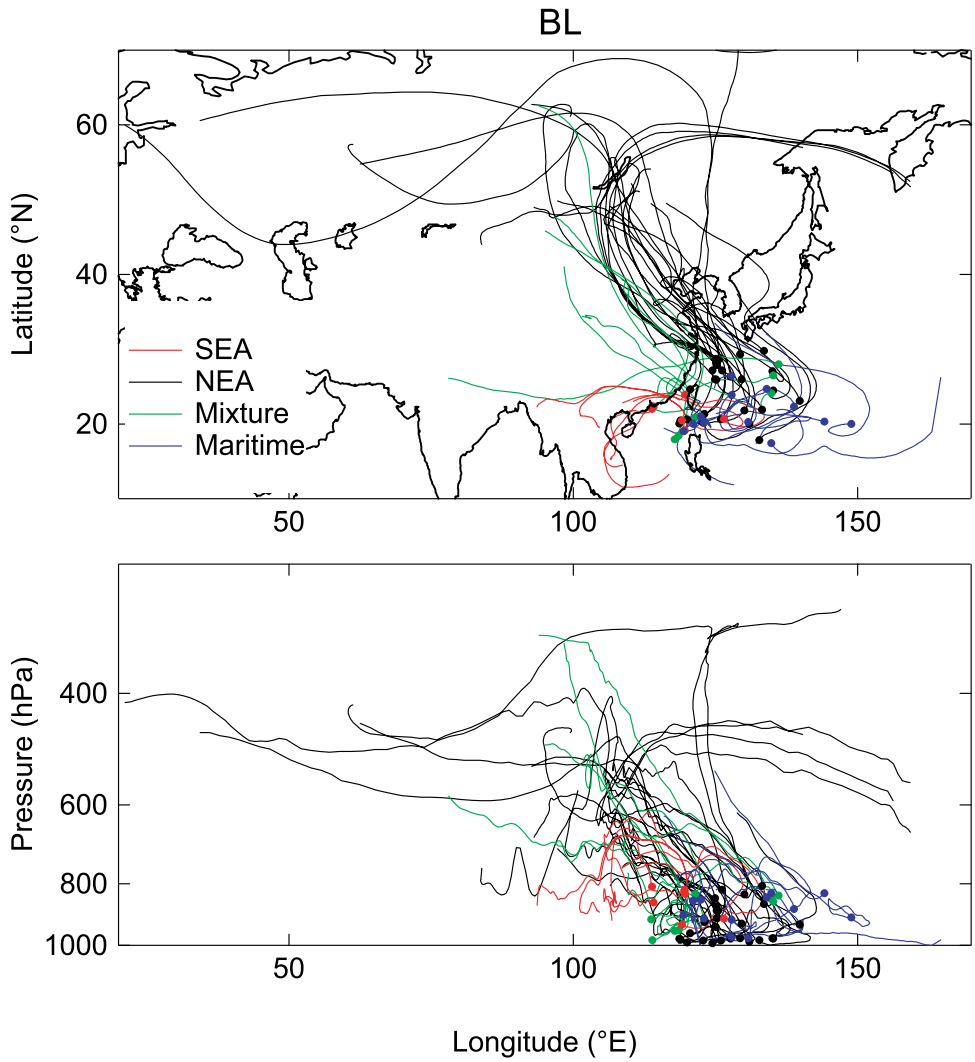

Figure 4a. Five-day back trajectories starting from the sampling point (closed circles) in the BL.

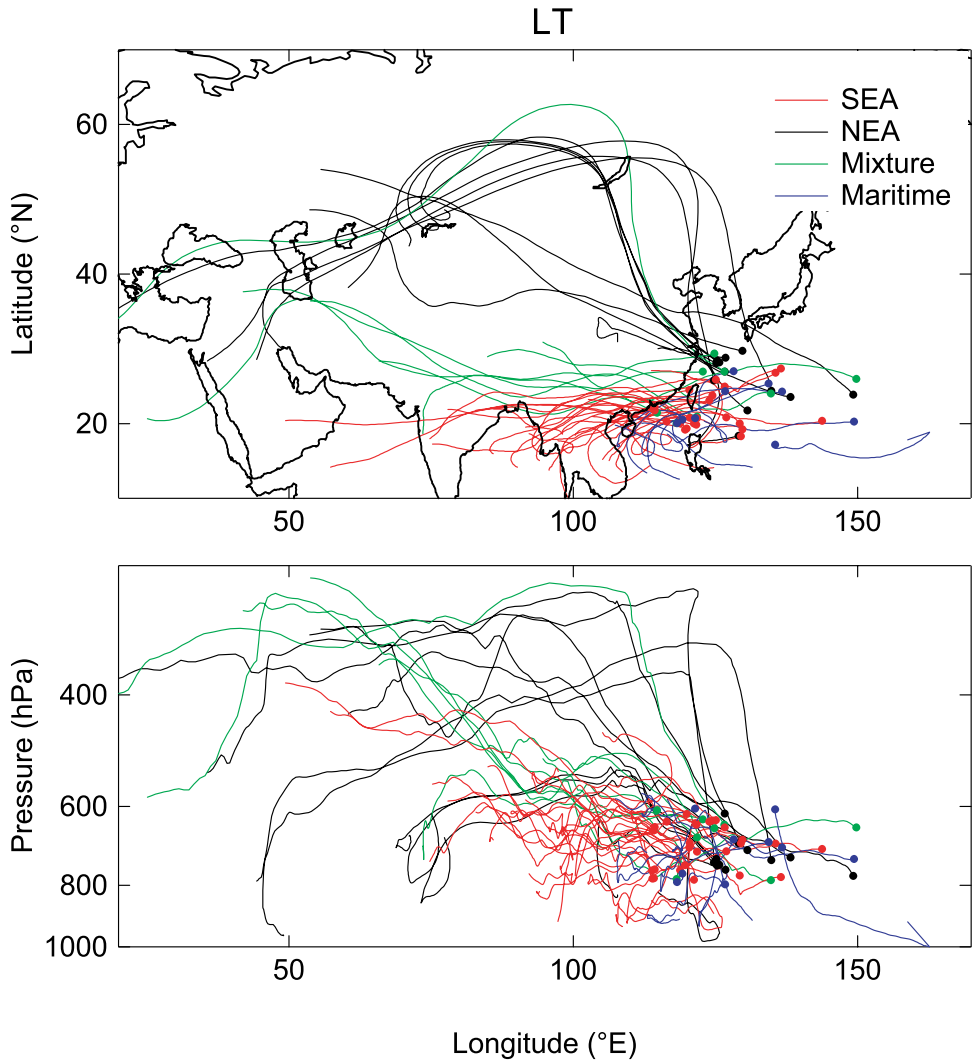

Figure 4b. Same as Figure 4a, but for the LT.

the Asian continent were classified as a mixture of SEA and NEA air masses. These air masses were excluded from the present analysis. Maritime air masses were transported from over the Pacific without passing over the Asian continent. They had remained in the study region for 5 days prior to being sampled. The probabilities of sampling different types of air masses changed with altitude. SEA air masses were dominant in the LT and MT, while NEA and maritime air masses were dominant in the BL, consistent with the C_2Cl_4 mixing ratios, discussed in section 3. The SEA air constitutes 15, 45, and 60% of the sampled air masses in the BL, LT, and MT, respectively. In the LT and MT, the dominant SEA air masses were transported from over peninsular SEA. Some of them had passed over northern India. In the MT, air from the tropical region (0°–10°N) was more frequently transported to the study region than in the LT, as seen in Figure 4b.

[14] Trajectories of SEA and maritime air masses were combined with the cloud heights determined by the GMS IR data to investigate the influence of convection on these air masses, as was done previously [*Miyazaki et al.*, 2002]. Most of the trajectories of air masses sampled below 4 km encountered convective clouds within 4 days prior to sampling, as shown in Figure 5. The probability of an encounter with convective clouds within 4 days decreased with altitude and reached 50% in the MT. However, most of the LT and MT trajectories do not show direct transport from the BL, although some of them show ascending motion due to convective transport, as shown in Figures 4b and 4c. Previous studies [e.g., *Kondo et al.*, 2002; *Miyazaki et al.*, 2002] have shown difficulties in accurately tracing air influenced by convection down to the BL with trajectories using 1.0°- or 2.5°- resolution meteorological data. The analyses of the cloud heights and trajectories indicate that a significant portion of the SEA air masses sampled in the LT were transported aloft from the BL over Southeast Asia by convection and therefore had chances to be impacted by biomass burning. This probability is lower in the MT, as discussed above.

[15] BL air from SEA was rarely transported to the sampling region without significant changes in altitude. Part of the LT and MT air aloft from the BL of SEA moved downward during eastward transport. Most of the SEA air masses sampled in the BL followed this pathway, as seen in Figure 4a.

[16] Most of the NEA air masses sampled in the BL were transported from Eurasia by strong northwesterly winds associated with the Siberian anticyclone and descended

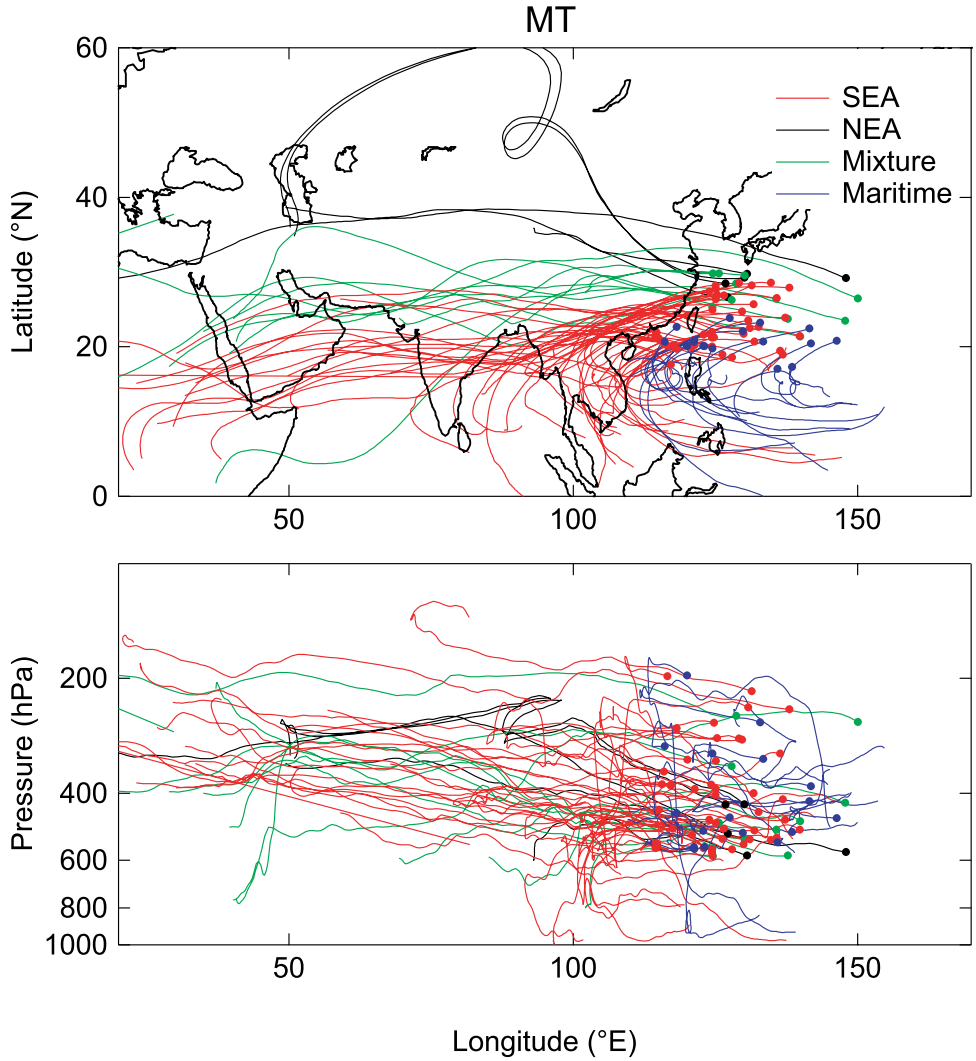

Figure 4c. Same as Figure 4a, but for the MT.

from the free troposphere down to the BL near the east coast of China around 25°–35°N (Figure 4a), suggesting the possible influence of northeastern China on these air masses, consistent with the chemical data shown in section 5.4.

5. Impact of Biomass Burning on Reactive Nitrogen and O_3

5.1. Vertical Profiles

[17] Profiles of the median values of O_3, CO, H_2O, CH_3Cl, C_2Cl_4, and the major components of reactive nitrogen (NO_x, PAN, HNO_3, NO_3^-, and NO_y) for each air mass type are shown in Figure 6. The data below 1 km are not shown because of the scarcity of the data. OH concentrations at fixed locations of observations were calculated with a photochemical time-dependent box model [*Davis et al.*, 1996; *Crawford et al.*, 1997] using the observed NO, O_3, H_2O, CO, NMHC, and $J(NO_2)$ values as input parameters. Diurnally averaged OH values were obtained and the median values are shown in Figure 6b.

[18] The CH_3Cl mixing ratios were similar in the maritime and NEA air, indicating that these air masses were not significantly impacted by biomass burning. The CH_3Cl

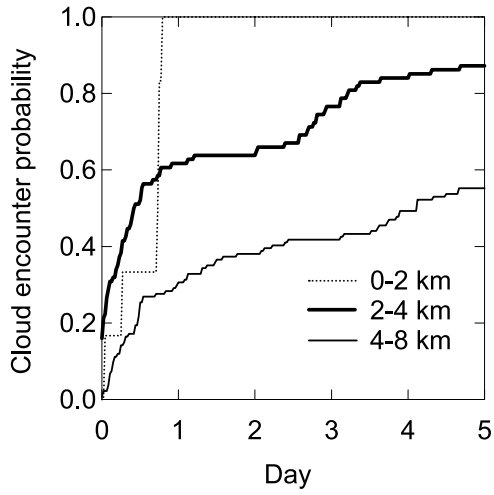

Figure 5. Probability of cloud encounter of air mass trajectories starting from the BL, LT, and MT as a function of elapsed time.

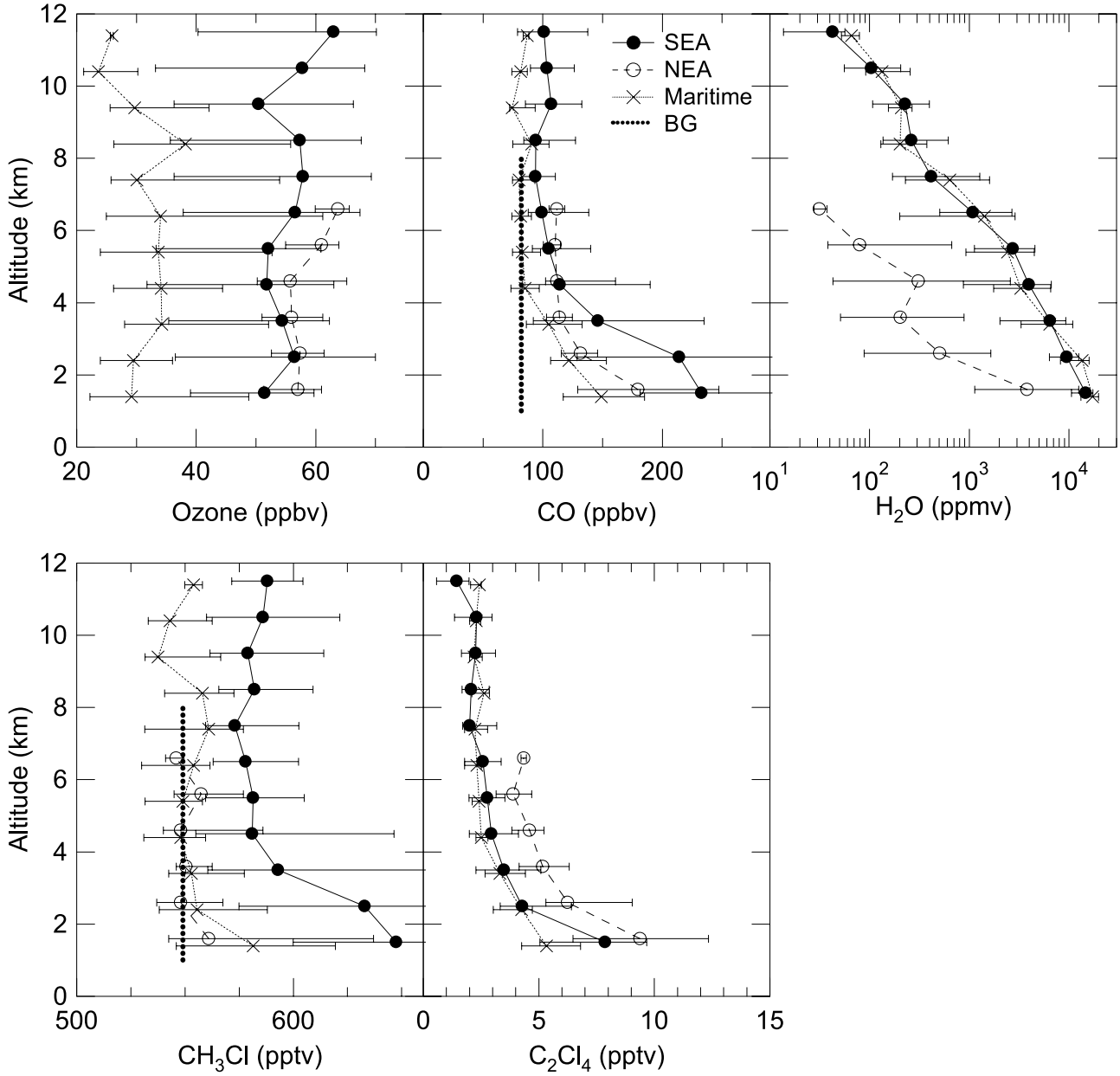

Figure 6a. Vertical profiles of the median mixing ratios of O_3, CO, H_2O, CH_3Cl, and C_2Cl_4 in SEA, NEA, and maritime air. The bars indicate the central 67% values. The background values (BG) for CH_3Cl and CO are shown as dots.

values in these air masses therefore should be close to background values. By contrast, the CH_3Cl values in the SEA air were much higher than these values. The C_2Cl_4 values in the SEA air were similar to those in the maritime air at 2–11 km, indicating that SEA air was not significantly influenced by industrial activities.

[19] The mixing ratios of the other trace gases, except for H_2O and OH, were generally lowest in maritime air, reflecting a minimal influence of anthropogenic emissions on these air masses. OH concentration was highest in SEA air due to high humidity (Figure 6a), solar UV radiation, and NO (Figure 6b), which converts HO_2 to OH. The lifetimes of NO_x determined by the reaction $NO_2 + OH$ in the BL, LT, and MT are about 1 day, as summarized in Table 2, together with the median OH concentrations.

[20] The mixing ratios of O_3 and PAN in NEA air masses were similar to or somewhat higher than those in SEA air, despite the possible effect of biomass burning on the SEA air masses. The latitudinal gradient of these species over the western Pacific, relatively free from biomass burning influences [e.g., *Kawakami et al.*, 1997; *Kondo et al.*, 1997b, 2002], indicates the relative abundance between these air masses.

5.2. Biomass Burning Tracers

5.2.1. Background Level of CH_3Cl

[21] Background levels of the O_3 precursors for SEA air need to be determined in assessing the impacts of biomass burning emissions in SEA on these species. As a first step, the background level for CH_3Cl is determined using the

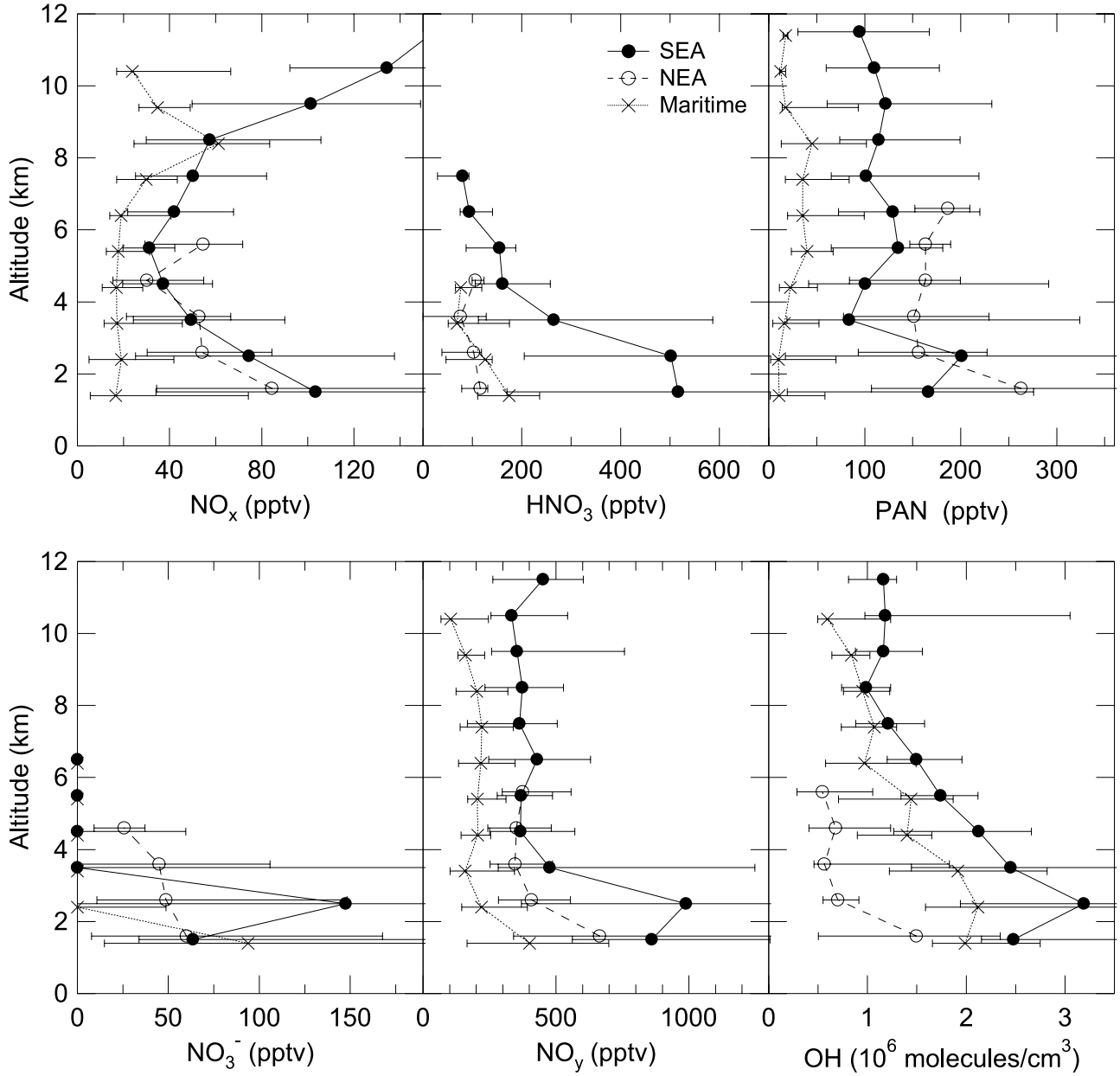

Figure 6b. Same as Figure 6a, but for NO_x, HNO_3, PAN, NO_3^-, NO_y, and OH (diurnal average).

correlation of C_2Cl_4 and CH_3Cl in SEA and NEA air masses, shown in Figure 7. In NEA air masses, C_2Cl_4 was enhanced independent of CH_3Cl due to the negligible impact of biomass burning. The median level of CH_3Cl in NEA was close to the lowest CH_3Cl levels in SEA air masses. Considering this, the background level of CH_3Cl for SEA air was determined to be the median CH_3Cl value of 549 (+17, −10; central 67%) pptv for the NEA air masses in the LT (shown as a thick line in Figure 7). The background level for the BL and MT air was assumed to be identical to that for the LT air (Figure 6a), considering that the lifetime of CH_3Cl is 1.3 years. The median value of CH_3Cl for NEA and maritime air masses in the BL was higher than the background level, suggesting the effect of mixing of these air masses with SEA air.

5.2.2. CO as a Biomass Burning Tracer

[22] Although CH_3Cl is a good parameter in representing the degree of primary emissions from biomass burning, intervals between sampling can be as long as 5 min. On the other hand, CO, which is also emitted by biomass burning, was measured every 1 s. Figure 8 shows correlations of CH_3Cl and C_2Cl_4 with CO in SEA air masses in the LT. CO was correlated very well with CH_3Cl at all altitudes (r^2 = 0.87). Correlation of CO with C_2Cl_4 was poorer, especially in the LT (r^2 = 0.22). The slope of the CH_3Cl-CO correlation ($\Delta CH_3Cl/\Delta CO$) was 0.58 pptv/parts per billion by volume (ppbv), similar to the estimated emission ratio (ER) of 0.64 pptv/ppbv for biomass burning in savanna regions. The ER for tropical forest is estimated to vary significantly in the range of 0.11–0.96 pptv/ppbv [*Andreae and Marlet*, 2001]. The background level for CH_3Cl can be

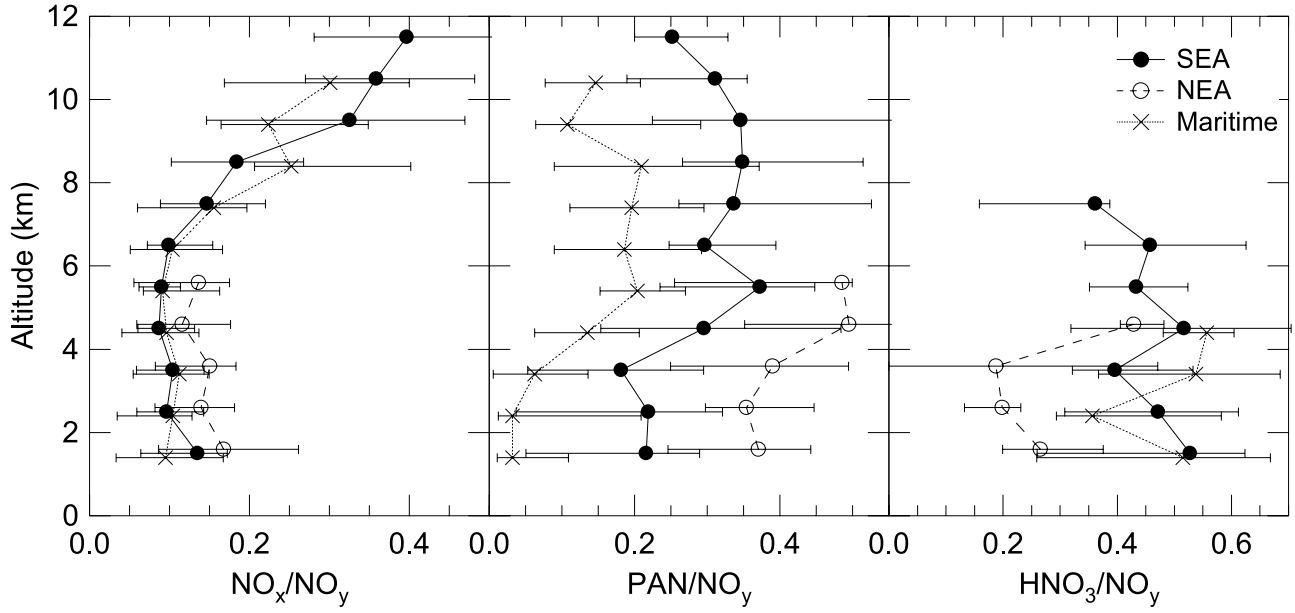

Figure 6c. Same as Figure 6a, but for NO_x,/NO_y, PAN/NO_y, and (HNO_3 + NO_3^-)/NO_y, ratios.

transformed to the corresponding CO values using the CH_3Cl-CO correlation in SEA air. The resulting CO background level in the LT was determined to be 82 (+28, −17; central 67%) ppbv, as shown in Figure 6a. The background level for CO in the MT and BL was assumed to be the same as in the LT, similarly to CH_3Cl. The median values of CO in the NEA and maritime air masses are similar to the background value in the LT and MT, but are considerably higher in the BL.

[23] Although the C_2Cl_4-CO correlation is poor, correlation is positive (slope = 0.0091 pptv/ppbv), suggesting some effect of mixing of SEA air with air masses influenced by industrial activity. This point is discussed in a quantitative way in section 5.6.

5.3. SEA Air

[24] For the discussion of production and loss of reactive nitrogen and O_3 made in this section and section 5.7, correlations of these species with CO are used.

5.3.1. O_3

[25] Correlations of O_3 with CO in the BL, LT, and MT of the SEA and NEA air masses are shown in Figure 9. The data with H_2O mixing ratios lower than 4000 parts per million by volume (ppmv) are shown as blue dots. It has been found that the square of the correlation coefficient (r^2) and the slope (S) for the O_3-CO correlation in the LT and MT for SEA air reached maxima by excluding data with H_2O < 4000 ppmv, after varing the H_2O threshold between 0–8000 ppmv. The median H_2O mixing ratios were higher than 2000 ppmv below 6 km (Figure 6a). O_3-CO data with H_2O > 4000 ppmv constituted 78, 36 and 2% of the data obtained at 2–4, 4–6, and 6–8 km. It has been found that lowering the H_2O threshold below 4000 ppmv significantly degrades the O_3-CO correlation in the MT, indicating difficulty in quantitatively extracting signatures of biomass burning in dry air at 6–8 km. Five-day back trajectories indeed indicate that many of the dry air masses (H_2O < 4000 ppmv) were transported from higher altitudes (not shown). For subsequent analyses, only humid data (H_2O > 4000 ppmv) were used. Almost all the data at 6–8 km were rejected by this selection criterion. The O_3-CO correlation for SEA air masses is tight throughout the entire altitude range (r^2 = 0.61–0.77), and $\Delta O_3/\Delta CO$ in the LT and MT was similar (0.20 ppbv/ppbv).

Table 2. Lifetimes (τ) of NO_x and PAN in NEA and SEA Air

Type of Air	T, K	OH, 10^6 cm^{-3}	τ (NO_x), days	τ (PAN), days
NEA-BL	282	1.5	1.1	1.1
SEA-BL	288	2.5	0.7	0.5
SEA-LT	282	2.8	0.7	0.9
SEA-MT (4–6 km)	270	1.9	1.1	5.9

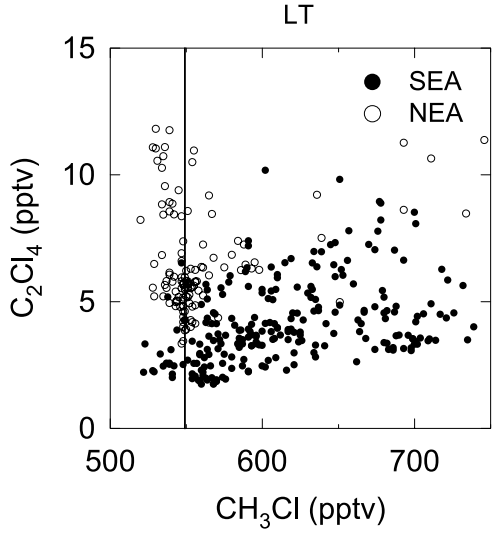

Figure 7. Correlation plot of C_2Cl_4 versus CH_3Cl in the LT of SEA and NEA air. The background CH_3Cl level for SEA was chosen to be the median of the CH_3Cl values for the NEA air (thick line).

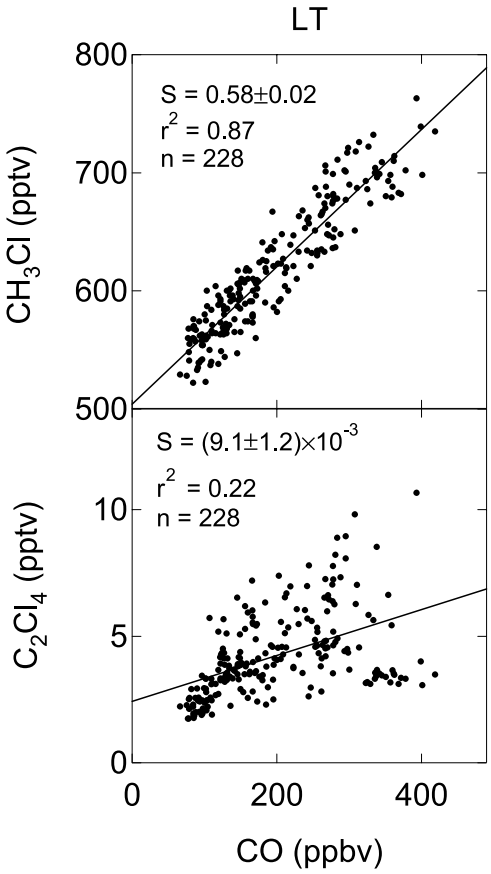

Figure 8. Correlation plots of CH_3Cl and C_2Cl_4 versus CO in the LT of SEA air. The regression line, slope (S), square of the correlation coefficient (r^2), and number of data (n) are also shown.

5.3.2. NO_x and PAN

[26] Correlations of NO_x, PAN, HNO_3, NO_3^-, NO_x + PAN, HNO_3 + NO_3^-, and NO_y with CO in the BL, LT, and MT of the SEA and NEA air are shown in Figures 10a and 10b for the observed CO range of 80–500 ppbv, together with the regression lines, slopes, and r^2. It should be noted here that for this analysis, only the data obtained on board the P-3B were used for HNO_3 and NO_3^-, as discussed in section 2. The dry SEA data (H_2O < 4000 ppmv) are shown as blue crosses.

[27] In the LT of SEA air, NO_x, PAN, NO_x + PAN, HNO_3, and NO_y were well correlated with CO, with r^2 = 0.54–0.80, demonstrating that biomass burning was the predominant source of reactive nitrogen in these air masses. The calculated median lifetime of PAN was about 1 day in the BL and LT, similar to that of NO_x. It increased to 6 days in the MT as summarized in Table 2, together with the median temperature used for the calculation. The lifetime of NO_x determined by the NO_2 + OH reaction during daytime will be shorter if hydrolysis of N_2O_5 on aerosols during nighttime is considered. The short lifetimes of NO_x and PAN should lead to conversion of NO_x + PAN to HNO_3 within 1–2 days. In fact, $\Delta(HNO_3 + NO_3^-)/\Delta CO$ was about 2 times larger than $\Delta(NO_x + PAN)/\Delta CO$ in the LT. Loss of NO_x + PAN must be compensated by the upward transport of biomass burning-impacted air rich in NO_x and PAN.

[28] NO_x continues to be oxidized while the rate of PAN decomposition slows at lower temperatures during upward transport from the LT to MT (Table 2). As a result, $\Delta NO_x/\Delta CO$ in the MT was smaller than that in the LT by a factor of 3. $\Delta PAN/\Delta CO$ changed little during upward transport, due to the chemical stability of PAN in the MT and its low solubility in water.

[29] The BL air was transported downward from the LT, as discussed in section 4. In the BL, $\Delta NO_x/\Delta CO$ in SEA air was comparable to that in the LT, suggesting sources of NO_x. The lifetime of PAN is as short as 0.5 days in the BL. The median NO_x production rate by PAN decomposition in the BL is calculated to be as high as 40 pptv $hour^{-1}$ for the median PAN values. Therefore the decomposition of PAN in the BL should significantly contribute to maintaining the high $\Delta NO_x/\Delta CO$ value in the BL.

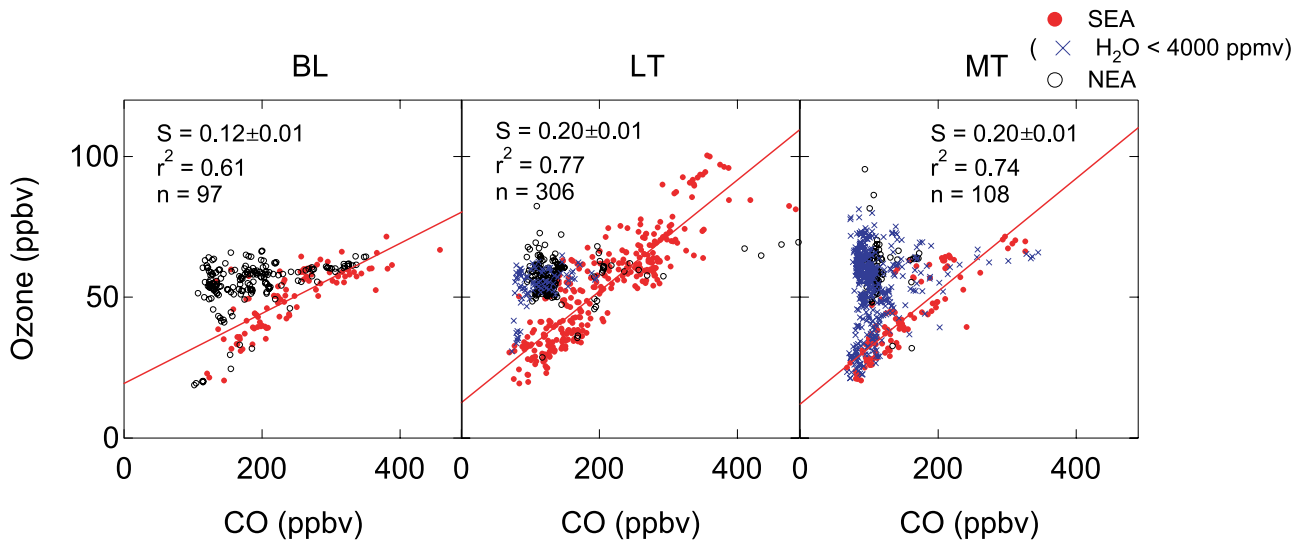

Figure 9. Correlation plots of O_3 versus CO in the BL, LT, and MT of SEA (red solid circles) and NEA (open circles) air. SEA data with H_2O < 4000 ppmv are shown as blue crosses. The number of the data (n) is for the data with H_2O > 4000 ppmv.

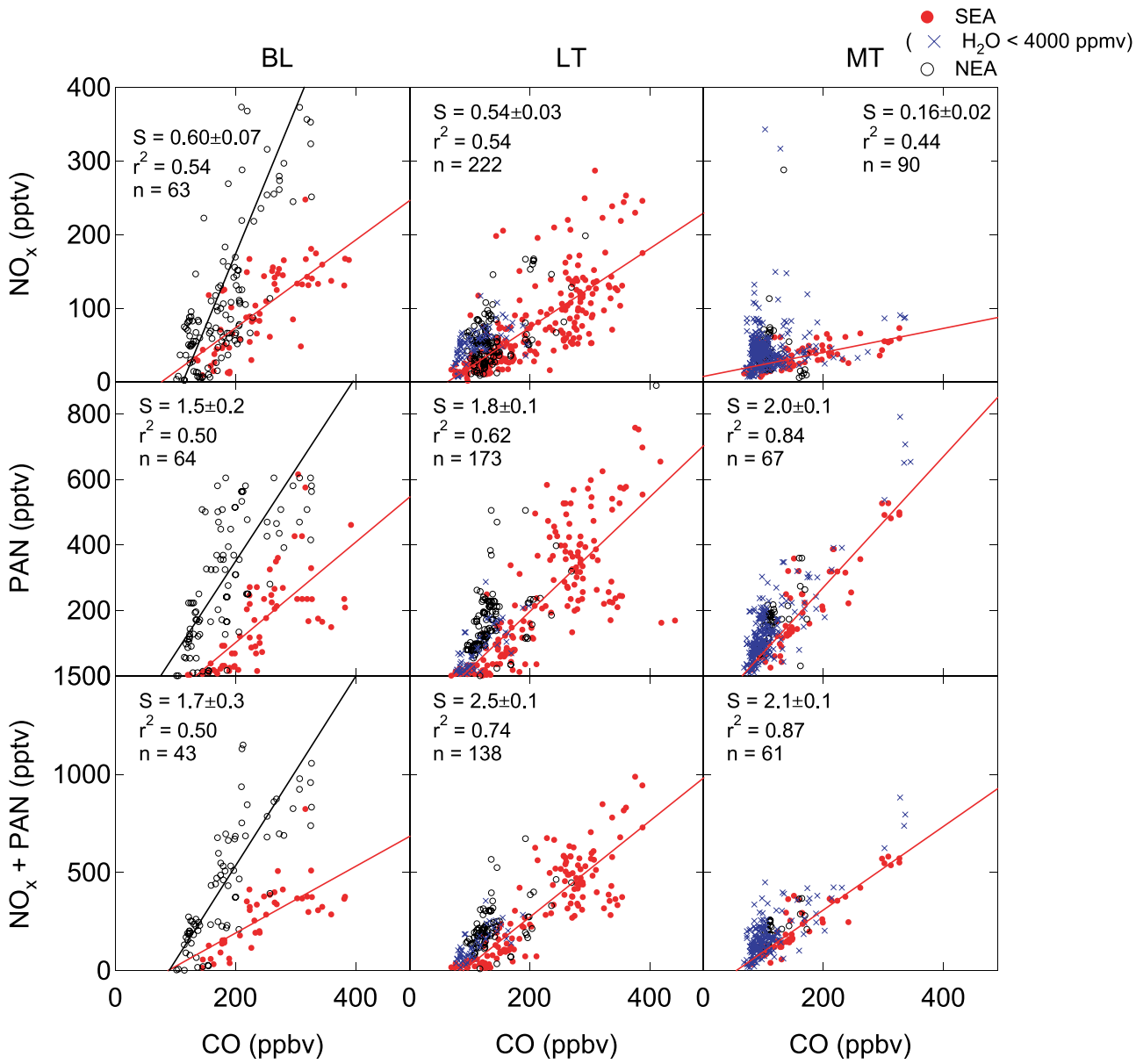

Figure 10a. Same as Figure 9, but for NO_x, PAN, and NO_x + PAN versus CO.

5.3.3. HNO_3, NO_3^-, and NO_y

[30] HNO_3 is produced by the oxidation of NO_x, as discussed in section 5.3.2. In the free troposphere, HNO_3 is removed by uptake by cloud droplets because of its high water solubility, followed by precipitation. Uptake by dust particles, followed by sedimentation, is another pathway of HNO_3 loss [e.g., *Song and Carmichael*, 2001; *Jordan et al.*, 2003]. HNO_3 also condenses on existing aerosols, which can be removed by precipitation after growing into cloud droplets. Nitrate measured on board the DC-8 includes particles larger than those on the P-3B, as discussed in section 2. Nitrate concentrations observed on the DC-8 were systematically higher than those observed on the P-3B in the BL of NEA, suggesting uptake of HNO_3 on coarse particles [*Jordan et al.*, 2003]. However, in SEA air, a majority of aerosol observed in the size range of 0.1–20 μm by the optical counter [*Clarke et al.*, 2004] was in the fine mode (less than 1 μm). Dominance of fine particles is typical for biomass burning plumes as observed, for example, in Brazil [*Reid and Hobbs*, 1998]. In addition, nitrate concentrations observed on the DC-8 and P-3B did not show any systematic difference (not shown), although the number of DC-8 observations was much smaller. These results indicate that in the SEA air, nitrate was abundant in the fine-mode aerosol but not in coarse particles and therefore the coarse particles were not an important sink of HNO_3. In the LT, the NO_3^- mixing ratio occasionally reached as high as 1000 pptv, which was close to the maximum gas-phase HNO_3 mixing ratio at a CO mixing ratio of 400 ppbv, indicating active conversion of HNO_3 into NO_3^-.

[31] $\Delta HNO_3/\Delta CO$ ($\Delta(HNO_3 + NO_3^-)/\Delta CO$) decreased from 3.5 (5.8) pptv/ppbv in the LT to 0.79 (1.2) pptv/ppbv in the MT. The change in the slope corresponds to a loss of

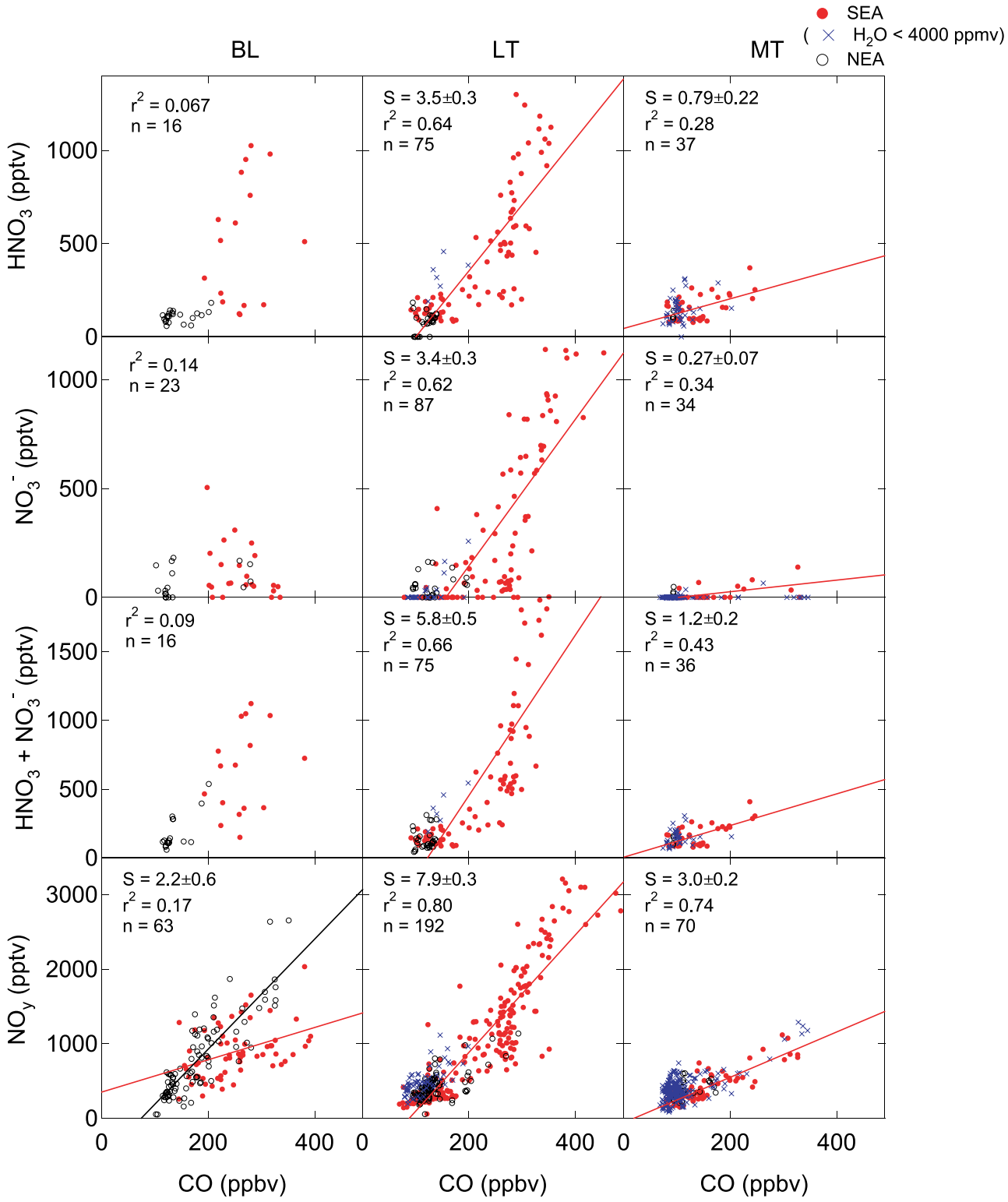

Figure 10b. Same as Figure 9, but for HNO_3, NO_3^-, $HNO_3 + NO_3^-$, and NO_y. The HNO_3 and NO_3^--data were obtained on board the P-3B.

HNO_3 ($HNO_3 + NO_3^-$) of 77% (79%). The NO_y-CO correlation is tighter than the ($HNO_3 + NO_3^-$)-CO correlation because NO_y is conserved to a greater degree than $HNO_3 + NO_3^-$. $\Delta NO_y/\Delta CO$ decreased from 7.9 pptv/ppbv in the LT to 3.0 pptv/ppbv in the MT, corresponding to a 62% loss of NO_y. This loss agrees well with the predicted NO_y decrease of 43% assuming an $HNO_3 + NO_3^-$ loss of 79% and an initial ($HNO_3 + NO_3^-$)/NO_y ratio in the LT of 0.45 (Figure 6). Removal of $HNO_3 + NO_3^-$ in the free troposphere should occur by precipitation during upward

Table 3. Estimated Annual Biomass Burning Emissions of NO_x, CO, and C_2H_4 in Southeast Asia[a]

	NO_x	CO	C_2H_4
Cambodia	62.20	1138	19.62
Laos	77.92	2352	46.99
Myanmar	162.84	6267	130.03
Thailand	189.26	5227	101.08
Vietnam	133.32	2917	52.65
Total	625.54 (±170%)	17901 (±156%)	350.37 (±164%)

[a]Units are in Gg. NO_x data are given as NO_2. Uncertainty exceeding 100%, for example, ±170% should be interpreted as "within a factor of 2.70," so that the confidence level would be 37–270% of the mean given.

transport. The altitude of water vapor saturation of the LT air was estimated assuming the H_2O and temperature profiles measured on board the P-3B and DC-8. Clouds are anticipated to form at about 4–5 km if the LT air masses continue to move upward adiabatically, consistent with the observed large loss of $HNO_3 + NO_3^-$ around this altitude. However, no quantitative relationship between the decreased H_2O and NO_y (or $HNO_3 + NO_3^-$) amounts was found. Although removal of H_2O should be associated with removal of HNO_3 in general, the rate of HNO_3 removal will not necessarily be proportional to that of H_2O. Efficient removal of HNO_3 has been shown to occur in tropical deep convection by calculations using a one-dimensional model [*Mari et al.*, 2000]. Mari et al. predicted that about 80% of HNO_3 is scavenged by warm and glaciated cloud, very similar to the present analysis.

[32] Transport efficiency ε (NO_y), defined as the average probability of transport of NO_y molecules from one region to another [*Koike et al.*, 2003; *Miyazaki et al.*, 2003], can be derived as the ratio of $\Delta NO_y/\Delta CO$ to the NO_x/CO ER, namely

$$\varepsilon(NO_y) = (\Delta NO_y/\Delta CO)/(NO_x/CO\ ER). \quad (1)$$

[33] The amounts of NO_x, CO, and C_2H_4 emitted per year from biomass burning in Thailand, Myanmar, Laos, Cambodia, and Vietnam have been estimated by *Streets et al.* [2003b] and are summarized in Table 3. Uncertainty exceeding 100% given in this table, for example ±170%, should be interpreted as "within a factor of 2.70," so that the confidence level would be 37–270% of the mean given. Biomass burning activity in Malaysia was weak during the March–April period according to the hot spot data from ATSR-2 (Figure 1) and was therefore excluded from these statistics. The annual emissions of NO_x, CO, and C_2H_4 by biomass burning in Malaysia are 9–14% of the total emissions in the five countries. The average $\Delta NO_y/\Delta CO$ of 7.9 pptv/ppbv in the LT is about 1/3 of the NO_x/CO ER of 21.3 pptv/ppbv (Table 3), suggesting an ε (NO_y) of 37% for biomass burning-impacted air. At CO mixing ratios lower than 300 ppbv, $\Delta NO_y/\Delta CO$ is 5.4 pptv/ppbv, which is 25% smaller than the average. The ε (NO_y) for the MT air decreased to 14%.

[34] The ε (NO_y) from the BL to the free troposphere over the western Pacific during the TRACE-P period was derived by *Koike et al.* [2003] and *Miyazaki et al.* [2003]. The ε (NO_y) from the East Asian BL to the LT and MT at 30°–42°N was statistically estimated by *Koike et al.* [2003] and

Table 4. Transport Efficiency of NO_y (ε (NO_y))[a]

Study Region	ER (NO_x/CO)	ε (NO_y) at 2–4 km	ε (NO_y) at 4–7 km
Present study (A): 17°–30°N	21	0.37	0.14
Present study (B): 17°–30°N	21	0.30	0.16
Koike et al. [2003]: 30°–42°N	53	0.10 ± 0.02	0.15 ± 0.03

[a]Emission ratios (ER) are given in pptv/ppbv. Present study (A): derived from $\Delta NO_y/\Delta CO$; (B): derived from $\delta NO_y/\delta CO$ (see text for details).

is compared with the present value in Table 4, together with the NO_x/CO ER. Major sources of NO_x and CO over the Asian continent at midlatitudes are estimated to be the combustion of fossil fuel and biomass. The LT value by Koike et al. is lower than the present value by a factor of 3, although the MT value is in good agreement. ε (NO_y) can depend on the oxidation rate of NO_x and the frequency and speed of upward transport. These different conditions and uncertainties controlling ε (NO_y) might have caused the difference in the LT.

5.4. NEA Air

[35] NEA air masses were most frequently sampled in the BL, and it is likely that they were influenced by emissions of pollutants from the coastal area of China, as suggested in section 4. In the BL, $\Delta NO_x/\Delta CO$, $\Delta PAN/\Delta CO$, and $\Delta NO_y/\Delta CO$ of the NEA air masses were much higher than those of the SEA air, demonstrating the distinct difference in the chemical characteristics of these air masses from SEA. $\Delta NO_y/\Delta CO$ of 13.5 pptv/ppbv is 2–6 times larger than that in the BL and LT of SEA air masses. However, the NO_x/CO ER for China for energy, industry, and agriculture is also as high as 64.1 pptv/ppbv, which is 3 times larger than that of 21.3 pptv/ppbv for biomass burning in SEA [*Streets et al.*, 2003a]. As a result, transport efficiency of NO_y within the BL is estimated to be 21%, assuming that most of the NO_y and CO were emitted over the coastal region of China.

[36] PAN mixing ratios at 1–2 km for NEA and SEA are plotted versus local temperature in Figure 11. In the NEA, higher PAN mixing ratios were observed at lower temperatures. The median temperature in the NEA air was lower than that in the SEA by 6 K (Table 2), indicating that PAN

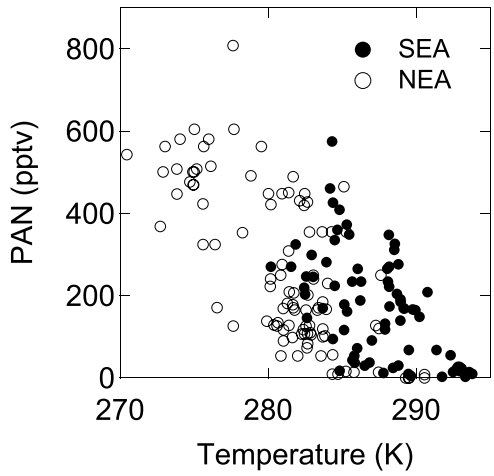

Figure 11. PAN mixing ratios versus temperatures at locations of measurements at 1–2 km for NEA (open circles) and SEA (closed circles) air.

Table 5. Background Values of O_3, CO, and Reactive Nitrogen for SEA Air

Species	0–2 km	2–4 km	4–8 km
O_3, ppbv	31	31	27
CO, ppbv	82	82	82
NO_x, pptv	17	17	20
HNO_3, pptv	89	89	89
NO_3^-, pptv	0	0	0
PAN, pptv	12	12	63
NO_y, pptv	240	240	225

in the NEA was formed over China, where temperatures were lower than those of the sampling regions. The median lifetime of PAN in the BL for NEA air is about 1 day. NO_x can be efficiently produced by thermal dissociation of PAN, similarly to the SEA air. The lifetime of NO_x in NEA is somewhat longer than that in SEA due to the lower OH concentrations. This, combined with higher NO_x/CO ER and NO_x formation from PAN, contributes to the high $\Delta NO_x/\Delta CO$ in NEA air.

5.5. Assessment of Biomass Burning Impacts on O_3 and Its Precursors

[37] Increases in the mixing ratios of O_3 and its precursors from biomass burning emissions in humid (H_2O > 4000 ppmv) SEA air masses are assessed by defining their background levels in the same way as was done for CO in section 5.2. For this purpose, the threshold for CO was determined to be 110 ppbv = 82 (background) + 28 (upper central 67%) ppbv for all altitudes. The background levels X^B of a species X in the LT and MT were defined as the median values of the mixing ratios in air masses with CO concentrations lower than this threshold and are listed in Table 5. Because there were little or no data with CO below 110 ppbv in the BL, X^B for these species were assumed to be the same as those in the LT. Similarly, the impacted value X was defined as the median value of the mixing ratios in air masses with CO concentrations higher than 110 ppbv. The net increase $\delta X = X - X^B$ and X^B are summarized in Table 6. ε (NO_y) can also be derived from $\delta NO_y/\delta CO$, and the derived values are compared with those derived from $\Delta NO_y/\Delta CO$ in Table 4. Both ε (NO_y) values are very similar, indicating the consistency of the present analysis.

[38] CO is emitted directly from biomass burning and is largely conserved prior to sampling because of its lifetime of about 18 days in the LT. Although NO_y is also directly emitted, it undergoes removal. It can be seen from Figures 6a and 6b and Tables 4 and 5 that the impact of biomass burning on NO_y was greatest in the LT with δNO_y = 810 pptv. δPAN and δHNO_3 made comparable contributions to δNO_y, and the sum of these constituted 70% of δNO_y (250 pptv). The rest of δNO_y was due to δNO_x and δNO_3^-.

[39] The observed PAN values in the BL and LT were due almost entirely to biomass burning because the background level for PAN was very low. In the MT, δPAN = 180 pptv and contributed to 70% of δNO_y. By contrast, δNO_x and δHNO_3 were small, demonstrating the important role of PAN in the long-range transport of reactive nitrogen emitted by biomass burning.

Table 6. Median Values of O_3, CO, and Reactive Nitrogen in SEA Air With CO > 110 ppbv[a]

Species	0–2 km	2–4 km	4–8 km
O_3, ppbv	51 (20)	57 (26)	45 (18)
CO, ppbv	233 (151)	209 (127)	158 (76)
NO_x, pptv	106 (89)	72 (55)	36 (16)
HNO_3, pptv	517 (428)	445 (356)	158 (69)
NO_3^-, pptv	65 (65)	74 (74)	0 (0)
PAN, pptv	165 (153)	221 (209)	243 (180)
NO_y, pptv	854 (614)	1051 (811)	477 (252)

[a]The numbers in parentheses are the median values of the increase in the mixing ratio of species X above the background values (δX in the text).

5.6. Effect of Mixing

[40] The slight C_2Cl_4-CO correlation suggests some mixing of SEA air with air masses influenced by industrial activities (section 5.2.2). Patterns of fuel use in different sectors in SEA are similar to those in Japan and Korea [*Streets et al.*, 2003a]. The ratio of fuel use for industry (transport) to the total (=industry + transport + power generation) in SEA is 0.40 (0.31), which is similar to that of 0.32–0.38 (0.28–0.29) for Japan and Korea, where biomass burning activity is very low. This suggests that C_2Cl_4-CO correlation in plumes influenced by emissions from Japan or Korea is a good reference for the correlation impacted by industrial activities (industry, transport, and power generation) in SEA. C_2Cl_4-CO correlations strongly influenced by industrial/urban emissions were obtained at 0–3 km over the western Pacific during other aircraft campaigns, namely, the Biomass Burning and Lightning Experiment (BIBLE)-B (September, 1999) [*Kondo et al.*, 2002] and Pacific Exploration of Asian Continental Emission (PEACE)-A (January 2002), and are shown in Figure 12. During these campaigns, outflow from Nagoya, Japan, and Pusan, Korea, was sampled. C_2Cl_4 was tightly correlated, especially in the Nagoya plumes (CO < 200 ppbv), and the average slope was 0.12 pptv/ppbv, which is 13 times larger than that for SEA air. From this, the degree of mixing of air masses influenced by industrial activities on observed CO is estimated to be about 8%.

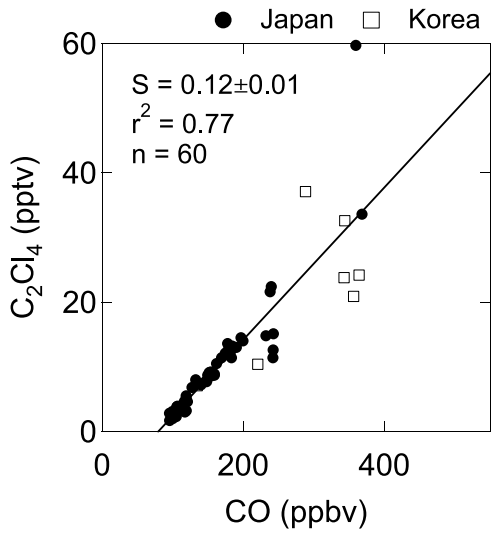

Figure 12. C_2Cl_4–CO correlation observed in the urban plumes from Japan and Korea sampled at 0–3 km during BIBLE-B (September–October) and PEACE-A (January) aircraft campaigns.

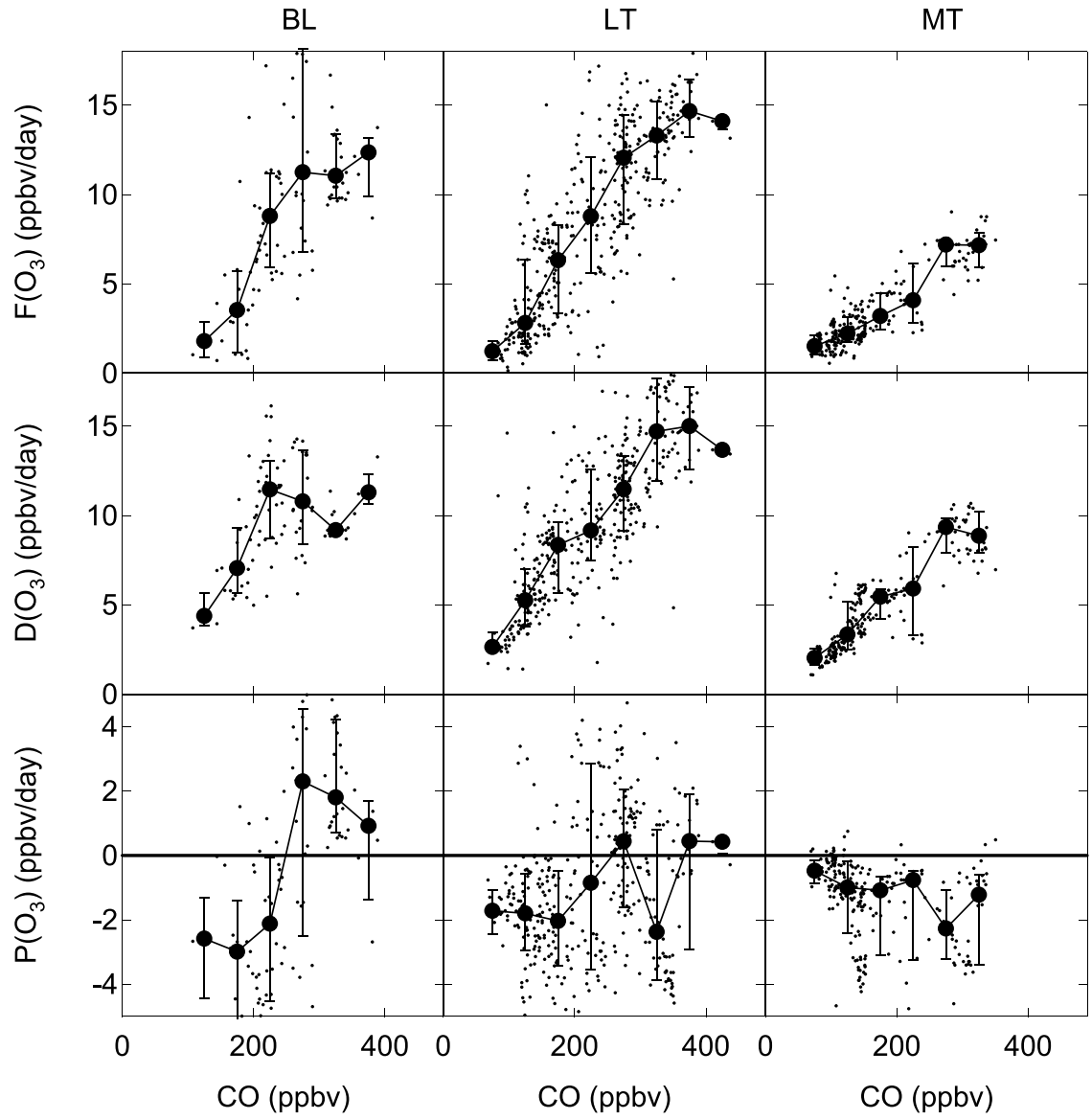

Figure 13. O_3 formation rate (F), destruction rate (D), and net O_3 production rate (P = F − D) as a function of CO in the BL, LT, and MT.

[41] The fractions of CO and NO_x emitted by biomass burning to the total amounts per year in SEA are estimated to be 55 and 35%, respectively [*Streets et al.*, 2003a, 2003b]. About 46 ± 10% of CO and NO_x emissions by biomass burning occur in March (Figure 1) [*Streets et al.*, 2003b]. Assuming that there is no seasonal variation in the industrial emissions, the contribution of biomass burning to the total emissions in March is estimated to be 87 and 75% for CO and NO_x, respectively. Contributions of industrial activities to the CO and NO_x mixing ratios observed in SEA plumes are estimated to be 1–2%, considering 8% mixing of industrial plumes.

[42] The effect of mixing on the O_3-CO correlation should be smaller than that on the NO_x-CO correlation. Most of the O_3 is likely produced within the lifetime of NO_x (shorter than 1 day; Table 2). Therefore NO_x produced by industrial activities will not directly influence O_3 production in biomass burning plumes because the two regions are well separated geographically, in general. The O_3-CO correlation in the industrial plumes may alter the O_3-CO correlation in the biomass burning plumes by mixing if they are very different. As discussed in the next section, the slope of the O_3-CO correlation in the urban plumes over the United States and Europe agrees with that in the biomass burning plumes to within a factor of 2. Therefore the partial mixing of industrial plumes should not strongly impact the O_3-CO correlation for biomass burning plumes in SEA.

5.7. O_3 Production

[43] The similarity in the $\Delta O_3/\Delta CO$ in the LT and MT suggests that O_3 was not produced during transport from the LT to MT. In order to investigate locations of O_3 production in the biomass burning plumes, we calculated photochemical formation (F), destruction (D), and net production (P = F − D) rates using the same box model as that used for OH calculation, as shown in Figure 13. For

Table 7. $\Delta O_3/\Delta CO$, Emission Ratios (ER), and Ozone Production Efficiency (OPE) for Biomass Burning, Urban, and Petrochemical Plumes[a]

Location	Reference	$\Delta O_3/\Delta CO$	Altitude, km	Age, days	ER (NO_x/CO)	ER (C_2H_4/NO_x)	OPE
Present study	1, 2	0.20 (±5%)	2–8	2–3	21 (±231%)	0.92 (±234%)	9.5 (±231%)
Australia	3, 4	0.12 (±3%)	1–3	0.5–3	18 (±10%)	0.38 (±10%)	6.7 (±30%)
South Africa	5	0.22 (±5%)[b]	1–6	2–4	44 (±36%)	0.38 (±35%)	5.0 (±36%)
Canada	6, 7	0.10 (±5%)[b]	1–3	3–4	7 (±54%)	1.57 (±87%)	15.7 (±54%)
United States and Europe	8, 9, 10, 11, 12	0.35 (±15%)	0	0.3	170 (±40%)	0.073 (±30%)	2.1 (±50%)
Houston, Texas	13			0.2		3.6 (±17%)	17.9 (±50%)
Houston, Texas	13			0.2		1.5 (±17%)	10.3 (±50%)
Houston, Texas	13			0.1		2.4 (±17%)	10.9 (±50%)

[a]References: 1, *Andreae and Marlet* [2001]; 2, *Streets et al.* [2003a, 2003b]; 3, *Takegawa et al.* [2003b]; 4, *Shirai et al.* [2003]; 5, *Yokelson et al.* [2003]; 6, *McKeen et al.* [2002]; 7, *Wotawa and Trainer* [2000]; 8, *Chin et al.* [1994]; 9, *Parrish et al.* [1998]; 10, *Hirsch et al.* [1996]; 11, *Rickard et al.* [2002]; 12, *Parrish et al.* [2002]; 13, *Ryerson et al.* [2003]. ER (NO_x/CO) is given in pptv/ppbv, and ER (C_2H_4/NO_x) is given in pptv/pptv. OPE for Houston, Texas, was derived from $\Delta O_3/\Delta(NO_y - NO_x)$ (see text for details). Uncertainties in the estimates due to measurement errors and natural variability (1-σ) are given where available.

[b]These numbers are assumed to be the same as the present study.

the region of this study, diurnally averaged F and D terms are expressed as

$$F(O_3) = (k_{NO+HO2}[HO_2] + k_{NO+RO2}[RO_2])[NO] \quad (2)$$

$$D(O_3) = k_{H2O+O(1D)}[O(^1D)][H_2O] + (k_{O3+OH}[OH] + k_{O3+HO2}[HO_2])[O_3], \quad (3)$$

where RO_2 represents peroxy radicals (e.g., CH_3O_2), [X] is the number density of species X, and k_{X+Y} is the reaction rate coefficient for the X + Y reaction. The F and D values increase linearly with NO and O_3, respectively (equations (2) and (3)). F increased with CO in the LT and MT, because NO_x and therefore NO increased with CO (Figure 10a). The D values also increased linearly with CO, because O_3 increased with CO. As a result, the F - D values were close to zero or slightly negative in the LT and MT, consistent with the similarity of $\Delta O_3/\Delta CO$ in the LT and MT. This tendency is typical for low-latitude air. At 5°–25°N, the median P values at 0–8 km were negative or close to zero for the whole data set sampled during TRACE-P [*Davis et al.*, 2003]. By contrast, at 25°–45°N, the median P values were positive. The lower P values at lower latitudes in March are mainly due to higher H_2O, which destroys O_3 (equation (3)). From these results, it is very likely that most of the enhanced O_3 in the biomass burning plumes was produced before transport to the sampling regions.

5.7.1. O_3 Production Efficiency

[44] The $\Delta O_3/\Delta CO$ for SEA air masses is compared with that obtained in other subtropical and boreal burning regions and is summarized in Table 7. The data over northern Australia were obtained in the boundary layer (<3 km) during BIBLE-B in September [*Takegawa et al.*, 2003b]. The data in Africa were obtained at 0.5–6 km during the Southern African Regional Science Initiative 2000 (SAFARI 2000) [*Hobbs et al.*, 2003; *Yokelson et al.*, 2003]. The $\Delta O_3/\Delta CO$ value of 0.22 for SAFARI 2000 was measured in biomass burning haze 2–4 days old off the coast of Namibia [*Yokelson et al.*, 2003].

[45] It is remarkable that the $\Delta O_3/\Delta CO$ values in fire plumes in different subtropical regions after 0.5–4 days following emission are similar to within a factor of 2, considering the possible variability in the conditions for photochemical O_3 production and loss by deposition. In the measurements over northern Australia and Africa, buildup of O_3 occurred near the fires within a half day, before O_3 precursors (such as NO_x and NMHCs) were consumed and diluted. $\Delta O_3/\Delta CO$ remained nearly constant during transport in the BL over northern Australia for a few days [*Takegawa et al.*, 2003b], supporting comparison of $\Delta O_3/\Delta CO$ observed in air masses with different ages. In order to understand this similarity in terms of photochemistry, we estimated the net number of O_3 molecules produced per NO_x molecule oxidized (or emitted), known as the O_3 production efficiency (OPE). The notion of OPE was first introduced by *Liu et al.* [1987] to estimate O_3 formation rates over the U.S. continent. Here OPE (net number of O_3 molecules produced per NO_x molecule emitted) has been derived by dividing $\Delta O_3/\Delta CO$ by NO_x/CO ER, as was done by *Chin et al.* [1994]. The NO_x/CO ER and OPE are given in Table 7. The NO_x/CO ER and C_2H_4/CO ER for SEA were derived from the sum of emissions of NO_x, CO, and C_2H_4 by the burning of savanna/grasslands, forest, and crop residue in the five SEA countries (Table 3). The ERs for other regions are based on in situ measurements in fresh plumes. OPE is controlled by NMHC concentrations at high NO_x levels (hydrocarbon-limited) [e.g., *Liu et al.*, 1987; *Sillman et al.*, 1990]. C_2H_4 is one of the major NMHCs emitted from biomass burning [e.g., *Shirai et al.*, 2003, and references therein; *Yokelson et al.*, 2003] and is an important precursor for efficient O_3 production. The average OPE for savanna fires is 7.1 ± 2.4.

[46] Air masses impacted by the Canadian forest fires were transported southward and sampled at 1–3 km over the southeastern United States in July during the 1995 Southern Oxidants Study (SOS-95) [*Wotawa and Trainer*, 2000; *McKeen et al.*, 2002]. The $\Delta O_3/\Delta CO$ for the Canadian forest fires, together with the other parameters, is summarized in Table 7. The OPE for the Canadian fires was 2 times larger than the average value for the subtropical fires. For these fires, the C_2H_4/NO_x ER was 2–3 times larger and the NO_x/CO ER was 2–6 times smaller than those for the Savanna fires.

[47] OPE was also derived by using $\Delta O_3/\Delta(NO_y - NO_x)$ for urban plumes [e.g., *Chin et al.*, 1994; *Hirsch et al.*, 1996; *Rickard et al.*, 2002, and references therein] to estimate the net number of O_3 molecules produced per NO_x molecule oxidized. It is known that OPE estimated

by using $\Delta O_3/\Delta CO$ is lower than that estimated by using $\Delta O_3/\Delta(NO_y - NO_x)$ [e.g., *Chin et al.*, 1994; *Hirsch et al.*, 1996; *Ryerson et al.*, 2001; *Rickard et al.*, 2002, and references therein]. Deposition of HNO_3, which constitutes a major fraction of $NO_y - NO_x$, leads to overestimates of OPE by the use of $\Delta O_3/\Delta(NO_y - NO_x)$. On the other hand, the OPE derived using $\Delta O_3/\Delta CO$ should be considered a lower limit because O_3 is negatively correlated with CO due to deposition of O_3 in the absence of photochemistry [*Chin et al.*, 1994]. The values of $\Delta O_3/\Delta CO$, ERs, and OPE for urban plumes in the United States are given in Table 7 for comparison. $\Delta O_3/\Delta CO$ was a uniform 0.3 at nonurban sites in eastern North America in summer [*Chin et al.*, 1994]. It was also uniform at 0.3–0.4 in the summer in Atlantic Canada and the spring in the Azores [*Parrish et al.*, 1998]. NO_x/CO ER was estimated to have increased linearly from 140 ± 60 pptv/ppbv in 1990 to 200 ± 80 pptv/ppbv in 2000 [*Parrish et al.*, 2002; D. D. Parrish, unpublished results, 2003]. C_2H_4/NO_x ER was derived from the National Acid Precipitation Assessment Program (NAPAP) inventory for the United States in 1995 [*Saeger et al.*, 1989] and the U.S. Environment Protection Agency report for 2003 (http://www.epa.gov/ttn/chief) (D. D. Parrish, unpublished results, 2003). The OPE for urban plumes is lower by a factor of 2–4 than that for biomass burning plumes despite the higher $\Delta O_3/\Delta CO$ ratio. This is due to a much higher NO_x/CO ER and a much lower C_2H_4/NO_x ER, which is typical for fossil fuel combustion at high temperatures. High NO_x with an insufficient supply of NMHCs reduces OPE, as observed in power plant plumes [*Ryerson et al.*, 2001].

[48] Measurements of OPE were made using $\Delta O_3/\Delta(NO_y - NO_x)$ in plumes strongly impacted by petrochemical emissions of alkenes in the Houston, Texas, metropolitan area in August [*Ryerson et al.*, 2003]. The plume ages were 1–4 hours. Because NO_y was nearly conserved in these plumes, the effect of HNO_3 deposition on OPE was small. It was shown that C_2H_4 and C_3H_6 promoted the rapid buildup of O_3 within 4 hours. The resulting OPEs of 10–18 in these plumes were much higher than those in urban plumes (about 2) because of much higher concentrations of these alkenes, which rapidly react with OH, efficiently producing HO_x. OPE was shown to increase with the C_2H_4/NO_x and C_3H_6 ER in these plumes. These data are also listed in Table 7 for comparison.

[49] The OPE is plotted versus C_2H_4/NO_x ER for biomass burning (boreal and subtropical fires), urban, and petrochemical plumes in Figure 14. The OPE increases with C_2H_4/NO_x ER in biomass burning plumes as well as in urban-petrochemical plumes, although the slopes are somewhat different. The positive OPE-C_2H_4/NO_x ER correlations suggest that O_3 in the biomass burning plumes, as well as in urban plumes, was produced in hydrocarbon-limited regimes. Although more alkenes are available in biomass burning plumes than in urban plumes for the same amount of NO_x, major O_3 production occurs at locations where NO_x concentration is still high, as observed over northern Australia [*Takegawa et al.*, 2003b]. At these locations, the rate of O_3 production depends also on the concentrations of alkenes. The range of C_2H_4/NO_x ER for the petrochemical plumes partly overlaps with those for biomass burning. It is remarkable that the OPE for the petrochemical plumes in this C_2H_4/NO_x ER range agrees with those for

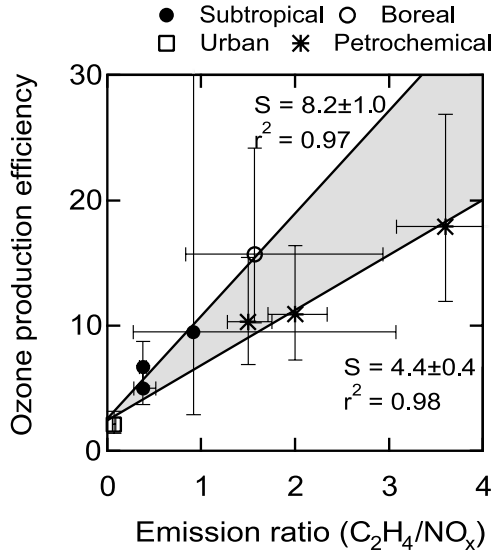

Figure 14. OPE as a function of C_2H_4/NO_x ER in biomass burning, urban, and petrochemical plumes.

biomass burning to within 50%. The difference of 50% is small considering the difference in the conditions for O_3 production, including differences in contributions of other NMHCs, H_2O concentration, solar actinic flux, air mass age, and boundary layer height. This similarity in the OPE demonstrates that C_2H_4/NO_x ER is a critical parameter that controls OPE in biomass burning plumes as well as fossil fuel combustion plumes. This result is understandable because C_2H_4 is the major constituent of highly reactive hydrocarbons both in biomass burning and urban emissions. In turn, improvement in the estimates of the emissions of C_2H_4 and C_3H_6 is critical in improving assessments of the effects of biomass burning on O_3.

5.7.2. O_3 Flux

[50] A net increase in the O_3 mixing ratio was assessed as shown in Table 6: in the BL, LT, and MT, δO_3 = 20, 26, and 18 ppbv, respectively. O_3^B decreased from 31 ppbv in the LT to 27 ppbv in the MT. Air transported from tropical latitudes was sampled more frequently in the MT, as discussed in section 4. The O_3^B of 31 ppbv is similar to the median O_3 value for maritime air shown in Figure 6, and $\delta O_3/O_3^B$ was 0.8 and 0.6 in the LT and MT, respectively. From these δO_3 values we have estimated the O_3 flux from SEA to the western Pacific caused by biomass burning. Air impacted by biomass burning was transported from SEA to the Pacific along westerlies, mostly at the latitude range of 17°–30°N, as seen from the wind vectors shown in Figure 3. O_3 flux across the meridional plane at 0–8 km along 120°E at 17°–30°N was calculated as

$$F(\delta O_3) = \int [\delta O_3 \times n_a \times U \times \eta \times f \times S]dz, \qquad (4)$$

where n_a is air number density, U is the average westerly component of the wind velocity given from the ECMWF data during TRACE-P, η is the probability of sampling the SEA air, excluding low-H_2O data, f is the fraction of the SEA data with CO > 110 ppbv, and S is the cross section of

Table 8. Parameters Used for Calculating the Net O_3 Flux[a]

	0–2 km	2–4 km	4–6 km	6–8 km
U, m/s	0.9 ± 5.0	8.7 ± 5.7	20.0 ± 10.3	27.4 ± 13.3
η	0.19 ± 0.11	0.40 ± 0.20	0.23 ± 0.22	0.01 ± 0.04
f	1.00 ± 0.00	0.91 ± 0.12	0.64 ± 0.33	1.00 ± 0.00

[a]U, average westerly component of the wind velocity; η, probability of sampling the SEA air masses excluding low-H_2O data; f, fraction of the data with CO > 110 ppbv.

the meridional plane. Because U increases with altitude (Figure 3), increases in O_3 at higher altitudes are more efficient in transporting O_3. These values at different altitudes are given in Table 8, together with the estimated uncertainties. η maximized in the LT and decreased with altitude. The O_3 flux in the BL was very small due to weak and unstable westerlies. The estimated $F(\delta O_3)$ is 50 (±133%) Gg O_3 day^{-1}.

[51] On the other hand, the total O_3 production rate over peninsular SEA can be derived independently, assuming that $\Delta O_3/\Delta CO$ is uniform (0.20 ppbv/ppbv) for all biomass burning-impacted air. The total CO emitted from SEA was estimated to be 17.9 (±155%) Tg CO yr^{-1} for the year of 2000 [*Streets et al.*, 2003b]. All of the SEA air masses used for the present analysis were sampled in March 2001. Considering that CO emissions in March constituted 46% (±22% relative error) of the total annual emission for 1997–2001 (Figure 1b), the emission rate in March is directly given as 267 (±157%) Gg CO day^{-1}. This is transformed to a total O_3 production rate of 73 (±157%) Gg O_3 day^{-1}. The $F(\delta O_3)$ derived above constitutes 68% (±206% relative error) of the estimated total O_3 production rate, suggesting that a majority of O_3 produced in SEA was transported to the western Pacific.

[52] In order to assess the overall accuracy of the derived O_3 flux, comparison was made with a value derived independently. O_3 fluxes in different types of air masses during TRACE-P were estimated using O_3 data obtained by lidar on board the DC-8 [*Browell et al.*, 2003]. Air masses characterized by high O_3 and low aerosol (HO3 category) in this study basically correspond to SEA air, and the O_3 flux of HO3 peaked at 26°N. The O_3 flux for HO3 air was integrated over the latitude range of 17°–30°N and an altitude range of 0–8 km resulting in 104 Gg O_3 day^{-1}. For comparison with this flux, δO_3 in equation (4) needs to be replaced with the median values of O_3 impacted by biomass burning (O_3).

$$F(O_3) = \int [O_3 \times n_a \times U \times \eta \times f \times S]dz. \quad (5)$$

The $F(\delta O_3)$ was estimated to be 114 (±135%) Gg O_3 day^{-1}, which is in reasonable agreement with that estimated by *Browell et al.* [2003], considering some differences in the sampling regions for the P-3B and DC-8 and in the criteria defining biomass burning-impacted air masses.

6. Conclusions

[53] Biomass burning activity was high over SEA (Thailand, Myanmar, Laos, Cambodia, and Vietnam) during the dry season of February–April 2001, when TRACE-P aircraft measurements were made. Convective activity over SEA, indicated by cloud images, frequently transported boundary layer air impacted by biomass burning to the free troposphere, followed by eastward transport to the sampling region over the western Pacific south of 30°N. As a result, air masses with enhanced CH_3Cl but low in C_2Cl_4 were frequently observed in the study region (17°–30°N, 110°–150°E). We selected air masses transported from the intense burning region south of 28°N using 5-day back trajectories and defined them as SEA air in order to evaluate the impact of biomass burning on O_3 and its precursors (CO and reactive nitrogen). NEA air masses were defined as those transported from north of 28°N over the Asian continent to the study region at 17°–30°N. The SEA air constitutes 15, 45, and 60% of the sampled air masses in the boundary layer (BL; 0–2 km), lower troposphere (LT; 2–4 km), and middle troposphere (MT; 4–8 km), respectively.

[54] CH_3Cl and CO, which were well correlated with HCN and CH_3CN, were chosen as primary and secondary tracers, respectively, to gauge the degree of impact of emissions of trace species from biomass burning. The impact of biomass burning was detectable from the O_3-CO correlation only in humid SEA air (H_2O > 4000 ppmv) below 6 km. Biomass burning has been found to be a predominant source of reactive nitrogen (NO_x, PAN, HNO_3, and nitrate) in this region from tight correlations of these species with CO (r^2 = 0.54–0.80) in the LT. Because of these tight correlations in the LT, we were able to quantify changes in the abundance of reactive nitrogen during upward transport based on changes in the slopes of the correlations.

[55] The lifetimes of NO_x and PAN were about 1 day in the BL and LT, due to the high OH concentrations and temperatures in SEA air. This led to rapid conversion of NO_x + PAN to HNO_3. Correspondingly, $\Delta(HNO_3 + NO_3^-)/\Delta CO$ was about 2 times greater than $\Delta(NO_x + PAN)/\Delta CO$ in the LT. About 80% of $HNO_3 + NO_3^-$ was removed by precipitation during upward transport from the LT to MT. $\Delta NO_x/\Delta CO$ decreased by a factor of 3 from the LT to MT due to continued oxidation and the lack of an additional supply of NO_x. $\Delta PAN/\Delta CO$ changed little due to the low water solubility of PAN and its long lifetime in the MT (about 6 days). The average $\Delta NO_y/\Delta CO$ of 7.9 pptv/ppbv was about 1/3 of the NO_x/CO ER of 21 pptv/ppbv for biomass burning in SEA, indicating the transport efficiency from the BL to the LT to be about 40%. Half of the NO_y remaining in the LT was lost during transport from the LT to MT. The loss of NO_y was due to the removal of $HNO_3 + NO_3^-$.

[56] Net increases in the mixing ratios of O_3 and its precursors were assessed by defining their background values using tracers. The net increases in O_3 and NO_y were largest in the LT, and their values were 26 ppbv and 810 pptv above the background values of 31 ppbv and 240 pptv, respectively. Increases in PAN and HNO_3 constituted a dominant part of the NO_y increase. In the MT, PAN made the largest contributions (180 pptv) to the NO_y increase (250 pptv), demonstrating its important role in the long-range transport of reactive nitrogen emitted by biomass burning.

[57] $\Delta O_3/\Delta CO$ of 0.20 ppbv/ppbv and an O_3 production efficiency (OPE) of 9.5 in the LT of SEA air were similar to

those in biomass burning plumes observed over northern Australia, Africa, and Canada/United States. C_2H_4 is one of the major NMHCs emitted from biomass burning and is an important precursor for efficient O_3 production. The OPE was positively correlated with C_2H_4/NO_x ER in the burning plumes. Major O_3 production occurs at locations where the NO_x concentration is still high, as observed in biomass burning plumes over northern Australia [*Takegawa et al.*, 2003b]. The OPE- C_2H_4/NO_x ER correlation suggests that the rate of O_3 production at these locations depends also on the concentrations of highly reactive NMHCs.

[58] C_2H_4 and C_3H_6 were elevated in the plumes strongly impacted by petrochemical emissions in Houston, Texas. The OPE values in these plumes and urban plumes were also correlated with C_2H_4/NO_x ER. In addition, these OPE values agree with those in the biomass burning plumes to within 50% at a C_2H_4/NO_x ER value of 1.5. These results demonstrate that major O_3 production proceeded in hydrocarbon-limited regimes in the biomass burning, urban, and petrochemical plumes and that the C_2H_4/NO_x ER was a critical parameter in determining OPE. These relationships should be useful in understanding and assessing the impact of biomass burning on O_3, including model studies.

[59] The net O_3 flux across the 120°E meridional cross-section at 17°–30°N was estimated to be 50 Gg O_3 day^{-1} in March. On the other hand, the total O_3 production rate in SEA was estimated to be 73 Gg O_3 day^{-1}, suggesting that about 70% of O_3 produced in SEA was transported to the western Pacific.

[60] **Acknowledgments.** We are indebted to all of the TRACE-P participants for their cooperation and support. Special thanks are due to the flight and ground crews of the NASA P3-B and DC-8 aircraft. We thank N. Toriyama and M. Kanada for their technical assistance with the measurements of NO_x and NO_y. The meteorological data were supplied by the European Center for Medium-Range Weather Forecasts (ECMWF). This work was supported in part by the Ministry of Education, Culture, Sports, Science, and Technology (MEXT) of Japan.

References

Andreae, M. O., and P. Marlet (2001), Emissions of trace gases and aerosols from biomass burning, *Global Biogeochem. Cycles*, *15*, 955–966.

Andreae, M. O., E. Atlas, H. Cachier, W. R. Cofer III, G. W. Harris, G. Helas, R. Koppmann, J.-P. Lacaux, and D. E. Ward (1996), Trace gas and aerosol emissions from savanna fires, in *Biomass Burning and Global Change*, edited by J. S. Levine, pp. 278–295, MIT Press, Cambridge, Mass.

Avery, M. D., J. Westberg, H. E. Fuelberg, R. E. Newell, B. E. Anderson, S. A. Vay, G. W. Sachse, and D. R. Blake (2001), Chemical transport across the ITCZ in the central Pacific during an El Nino-Southern Oscillation cold phase event in March–April 1999, *J. Geophys. Res.*, *106*, 32,539–32,553.

Blake, N. J., D. R. Blake, B. C. Sive, T. Y. Chen, F. S. Rowland, J. E. Collins, G. W. Sachse, and B. E. Anderson (1996), Biomass burning emissions and vertical distribution of atmospheric methyl halides and other reduced carbon gases in the South Atlantic region, *J. Geophys. Res.*, *101*, 24,151–24,164.

Blake, N. J., et al. (1999), Influence of southern hemispheric biomass burning on midtropospheric distributions of nonmethane hydrocarbons and selected halocarbons over the remote South Pacific, *J. Geophys. Res.*, *104*, 16,213–16,232.

Blake, N. J., et al. (2003), NMHCs and halocarbons in Asian continental outflow during the Transport and Chemical Evolution Over the Pacific (TRACE-P) field campaign: Comparison with PEM-West B, *J. Geophys. Res.*, *108*(D20), 8806, doi:10.1029/2002JD003367.

Bradshaw, J., et al. (1999), Photofragmentation two-photon laser-induced fluorescence detection of NO_2 and NO: Comparison of measurement with model results based on airborne observations during PEM-Tropics A, *Geophys. Res. Lett.*, *26*, 471–474.

Browell, E. V., et al. (2003), Large-scale ozone and aerosol distributions, air mass characteristics, and ozone fluxes over the western Pacific Ocean in late-winter/early-spring, *J. Geophys. Res.*, *108*(D20), 8805, doi:10.1029/2002JD003290.

Chan, C. Y., L. Y. Chan, H. Y. Liu, S. Christopher, S. J. Oltmans, and J. M. Harris (2000), A case study on the biomass burning in Southeast Asia and enhancement of tropospheric ozone over Hong Kong, *Geophys. Res. Lett.*, *27*, 1479–1482.

Chan, C. Y., L. Y. Chan, J. M. Harris, S. J. Oltmans, D. R. Blake, Y. Qin, Y. G. Zheng, and X. D. Zheng (2003), Characteristics of biomass burning emission sources, transport, and chemical speciation in enhanced springtime tropospheric ozone profile over Hong Kong, *J. Geophys. Res.*, *108*(D1), 4015, doi:10.1029/2001JD001555.

Chin, M., D. J. Jacob, J. W. Munger, D. D. Parrish, and B. G. Doddridge (1994), Relationship of ozone and carbon monoxide over North America, *J. Geophys. Res.*, *99*, 14,565–14,573.

Clarke, A. D., et al. (2004), Size-distributions and mixtures of black carbon aerosol in Asian outflow: Physiochemistry and optical properties, *J. Geophys. Res.*, *109*, D15S09, doi:10.1029/2003JD004378.

Crawford, J. H., et al. (1997), An assessment of ozone photochemistry in the extratropical western North Pacific: Impact of continental outflow during the late winter/early spring, *J. Geophys. Res.*, *102*, 28,469–28,487.

Crutzen, P. J., and M. O. Andreae (1990), Biomass burning in the tropics: Impact on atmospheric chemistry and biogeochemical cycles, *Science*, *250*, 1669–1678.

Davis, D. D., et al. (1996), Assessment of ozone photochemistry tendency in the western North Pacific as inferred from PEM-West A observations during the fall 1991, *J. Geophys. Res.*, *101*, 2111–2134.

Davis, D. D., et al. (2003), An assessment of western North Pacific ozone photochemistry based on springtime observations from NASA's PEM-West B [1994] and TRACE-P [2001] field studies, *J. Geophys. Res.*, *108*(D21), 8829, doi:10.1029/2002JD003232.

Dibb, J. E., R. W. Talbot, E. Scheuer, G. Seid, M. Avery, and H. Singh (2003), Aerosol chemical composition in Asian continental outflow during TRACE-P: Comparison to PEM-West B, *J. Geophys. Res.*, *108*(D21), 8815, doi:10.1029/2002JD003111.

Elvidge, C. D., and K. E. Baugh (1996), Survey of fires in Southeast Asia and India during 1987, in *Global Biomass Burning*, vol. 2, edited by J. Levine, pp. 663–670, MIT Press, Cambridge, Mass.

Fishman, J., J. M. Hoell Jr., R. D. Bendura, R. J. McNeal, and V. W. J. H. Kirchhoff (1996), NASA GTE TRACE-A experiment (September–October 1992): Overview, *J. Geophys. Res.*, *101*, 23,865–23,879.

Fuelberg, H. E., C. M. Kiley, J. R. Hannan, D. J. Westberg, M. A. Avery, and R. E. Newwell (2003), Atmospheric transport during the Transport and Chemical Evolution Over the Pacific (TRACE-P) experiment, *J. Geophys. Res.*, *108*(D20), 8782, doi:10.1029/2002JD003092.

Galanter, M., H. M. Levy II, and G. R. Carmichael (2000), Impacts of biomass burning on tropospheric CO, NO_x, and O_3, *J. Geophys. Res.*, *105*, 6633–6653.

Harriss, R. C., et al. (1988), The Amazon Boundary Layer Experiment (ABLE 2A): Dry season 1985, *J. Geophys. Res.*, *93*, 1351–1360.

Harriss, R. C., et al. (1990), The Amazon Boundary Layer Experiment (ABLE 2B): Wet season 1987, *J. Geophys. Res.*, *95*, 16,721–16,736.

Heald, C. L., D. J. Jacob, P. I. Palmer, M. J. Evans, G. W. Sachse, H. B. Singh, and D. R. Blake (2003), Biomass burning emission inventory with daily resolution: Application to aircraft observations of Asian outflow, *J. Geophys. Res.*, *108*(D21), 8811, doi:10.1029/2002JD003082.

Hinds, W. C. (1998), *Aerosol Technology*, 483 pp., John Wiley, Hoboken, N. J.

Hirsch, A. I., J. W. Munger, D. J. Jacob, L. W. Horowitz, and A. H. Goldstein (1996), Seasonal variation of the ozone production efficiency per unit NO_x at Harvard Forest, Massachusetts, *J. Geophys. Res.*, *101*, 12,659–12,666.

Hobbs, P. V., P. Sinha, R. J. Yokelson, T. J. Christian, D. R. Blake, S. Gao, T. W. Kirchstetter, T. Novakov, and P. Pilewskie (2003), Evolution of gases and particles from a savanna fire in South Africa, *J. Geophys. Res.*, *108*(D13), 8485, doi:10.1029/2002JD002352.

Hoell, J. M., D. D. Davis, D. J. Jacob, M. O. Rodgers, R. E. Newell, H. E. Fuelberg, R. J. McNeal, J. L. Raper, and R. J. Bendura (1999), Pacific Exploratory Mission in the tropical Pacific: PEM-Tropics A, August–September 1996, *J. Geophys. Res.*, *104*, 5567–5583.

Jordan, C. E., J. E. Dibb, B. E. Anderson, and H. E. Fuelberg (2003), Uptake of nitrate and sulfate on dust aerosols during TRACE-P, *J. Geophys. Res.*, *108*(D20), 8817, doi:10.1029/2002JD003101.

Kajii, Y., et al. (2002), Boreal forest fires in Siberia in 1998: Estimation of area burned and emissions of pollutants by advanced very high resolution radiometer satellite data, *J. Geophys. Res.*, *107*(D24), 4745, doi:10.1029/2001JD001078.

Kawakami, S., et al. (1997), Impact of lightning and convection on reactive nitrogen in the tropical free troposphere, *J. Geophys. Res.*, *102*, 28,367–28,384.

Keene, W. C., et al. (1999), Composite global emissions of reactive chlorine from anthropogenic and natural sources: Reactive chlorine emissions inventory, *J. Geophys. Res.*, *104*, 8429–8440.

Koike, M., et al. (2003), Export of anthropogenic reactive nitrogen and sulfur compounds from the East Asia region in spring, *J. Geophys. Res.*, *108*(D20), 8789, doi:10.1029/2002JD003284.

Kondo, Y., et al. (1997a), Performance of an aircraft instrument for the measurement of NO_y, *J. Geophys. Res.*, *102*, 28,663–28,671.

Kondo, Y., et al. (1997b), Profiles and partitioning of reactive nitrogen over the Pacific Ocean in winter and early spring, *J. Geophys. Res.*, *102*, 28,405–28,424.

Kondo, Y., et al. (2002), Effects of biomass burning, lightning, and convection on O_3, CO, and NO_y over the tropical Pacific and Australia in August–October 1998 and 1999, *J. Geophys. Res.*, *107*, 8402, doi:10.1029/2001JD000820. [printed *108*(D3), 2003]

Kondo, Y., et al. (2003), Uptake of reactive nitrogen on cirrus cloud particles in the upper troposphere and lowermost stratosphere, *Geophys. Res. Lett.*, *30*(4), 1154, doi:10.1029/2002GL016539.

Lindesay, J. A., M. O. Andreae, J. G. Goldammer, G. Harris, H. J. Annegarn, M. Garstang, R. J. Scholes, and B. W. van Wilgen (1996), International Geosphere-Biosphere Programme/International Global Atmospheric Chemistry SAFARI-92 field experiment: Background and overview, *J. Geophys. Res.*, *101*, 23,521–23,530.

Liu, H., D. J. Jacob, I. Bey, R. M. Yantosca, B. N. Duncan, and G. W. Sachse (2003), Transport pathways for Asian combustion outflow over the Pacific: Interannual and seasonal variations, *J. Geophys. Res.*, *108*(D20), 8786, doi:10.1029/2002JD003102.

Liu, S. C., M. Trainer, F. C. Fehsenfeld, D. D. Parrish, E. J. Williams, D. W. Fahey, G. Hübler, and P. C. Murphy (1987), Ozone production in the rural troposphere and the implications for regional and global ozone distributions, *J. Geophys. Res.*, *92*, 4191–4207.

Mari, C., D. J. Jacob, and P. Bechtold (2000), Transport and scavenging of soluble gases in a deep convective cloud, *J. Geophys. Res.*, *105*, 22,255–22,267.

McKeen, S. A., G. Wotawa, D. D. Parrish, J. S. Holloway, M. P. Buhr, G. Hübler, F. C. Fehsenfeld, and J. F. Meagher (2002), Ozone production from Canadian wildfires during June and July of 1995, *J. Geophys. Res.*, *107*(D14), 4192, doi:10.1029/2001JD000697.

Miyazaki, Y., K. Kita, Y. Kondo, M. Koike, M. Ko, W. Hu, S. Kawakami, D. R. Blake, and T. Ogawa (2002), Springtime photochemical ozone production observed in the upper troposphere over east Asia, *J. Geophys. Res.*, *107*, 8398, doi:10.1029/2001JD000811. [printed *108*(D3), 2003]

Miyazaki, Y., et al. (2003), Synoptic-scale transport of reactive nitrogen over the western Pacific in spring, *J. Geophys. Res.*, *108*(D20), 8788, doi:10.1029/2002JD003248.

Orsini, D., Y. Ma, A. Sullivan, B. Sierau, K. Baumann, and R. J. Weber (2003), Refinements to the particle-into-liquid sampler (PILS) for ground and airborne measurements of water-soluble aerosol chemistry, *Atmos. Environ.*, *37*, 1243–1259.

Parrish, D. D., M. Trainer, J. S. Holloway, J. E. Yee, M. S. Warshawsky, F. C. Fehsenfeld, G. L. Forbes, and J. L. Moody (1998), Relationships between ozone and carbon monoxide at surface sites in the North Atlantic region, *J. Geophys. Res.*, *103*, 13,357–13,376.

Parrish, D. D., M. Trainer, D. Hereid, E. J. Williams, K. J. Olszyna, R. A. Harley, J. F. Meagher, and F. C. Fehsenfeld (2002), Decadal change in carbon monoxide to nitrogen oxide ratio in U.S. vehicular emissions, *J. Geophys. Res.*, *107*(D12), 4140, doi:10.1029/2001JD000720.

Phadnis, M. J., and G. R. Carmichael (2000), Forest fire in the boreal region of China and its impact on the photochemical oxidant cycle of East Asia, *Atmos. Environ.*, *34*, 483–498.

Pochanart, P., J. Kreasuwun, P. Sukasem, W. Greeratithadaniyom, M. S. Tabucanon, J. Hirokawa, Y. Kajii, and H. Akimoto (2001), Tropical tropospheric ozone observed in Thailand, *Atmos. Envron.*, *35*, 2657–2668.

Pochanart, P., H. Akimoto, Y. Kajii, and P. Sukasem (2003), Carbon monoxide, regional scale transport, and biomass burning in tropical continental Southeast Asia: Observations in Thailand, *J. Geophys. Res.*, *108*(D17), 4552, doi:10.1029/2002JD003360.

Reid, J. S., and P. V. Hobbs (1998), Physical and optical properties of young smoke from individual biomass fires in Brazil, *J. Geophys. Res.*, *103*, 32,013–32,030.

Rickard, A. R., G. Salisbury, P. S. Monks, A. C. Lewis, S. Baugitte, B. J. Bandy, K. C. Clemitsshaw, and S. A. Penkett (2002), Comparison of measured ozone production efficiencies in the marine boundary layer at two European coastal sites under different pollution regimes, *J. Atmos. Chem.*, *43*, 107–134.

Ryerson, T. B., et al. (2001), Observations of ozone formation in power plant plumes and implications for ozone control strategies, *Science*, *292*, 719–723.

Ryerson, T. B., et al. (2003), Effect of petrochemical industrial emissions of reactive alkenes and NO_x on tropospheric ozone formation in Houston, Texas, *J. Geophys. Res.*, *108*(D8), 4249, doi:10.1029/2002JD003070.

Sachse, G. W., G. F. Hill, L. O. Wade, and M. G. Perry (1987), Fast response, high precision carbon monoxide sensor using a tunable diode laser absorption technique, *J. Geophys. Res.*, *92*, 2071–2081.

Saeger, M., et al. (1989), The 1985 NAPAN emissions inventory (version 2): Development of the annual data and modelers' tapes, *Rep. EPA-600/7-89-012a*, U.S. Environ. Prot. Agency, Washington D. C.

Shirai, T., et al. (2003), Emission estimates of selected volatile organic compounds from tropical savanna burning in northern Australia, *J. Geophys. Res.*, *108*(D3), 8406, doi:10.1029/2001JD000841.

Sillman, S., J. A. Logan, and S. C. Wofsy (1990), The sensitivity of ozone to nitrogen oxides and hydrocarbons in regional ozone episodes, *J. Geophys. Res.*, *95*, 1837–1851.

Singh, H. B., et al. (1996), Reactive nitrogen and ozone over the western Pacific: Distribution, partitioning, and sources, *J. Geophys. Res.*, *101*, 1793–1808.

Singh, H. B., et al. (2003), In situ measurements of HCN and CH_3CH over the Pacific Ocean: Sources, sinks, and budgets, *J. Geophys. Res.*, *108*(D20), 8795, doi:10.1029/2002JD003006.

Song, C. H., and G. R. Carmichael (2001), Gas-particle partitioning of nitric acid modulated by alkaline aerosol, *J. Atmos. Chem.*, *40*, 1–22.

Streets, D. G., et al. (2003a), An inventory of gaseous and primary aerosol emissions in Asia in the year 2000, *J. Geophys. Res.*, *108*(D21), 8809, doi:10.1029/2002JD003093.

Streets, D. G., K. F. Yarber, J.-H. Woo, and G. R. Carmichael (2003b), Biomass burning in Asia: Annual and seasonal estimates and atmospheric emissions, *Global Biogeochem. Cycles*, *17*(4), 1099, doi:10.1029/2003GB002040.

Takegawa, N., et al. (2003a), Removal of NO_x and NO_y in biomass burning plumes in the boundary layer over northern Australia, *J. Geophys. Res.*, *108*(D10), 4308, doi:10.1029/2002JD002505.

Takegawa, N., et al. (2003b), Photochemical production of O_3 in biomass burning plumes in the boundary layer over northern Australia, *Geophys. Res. Lett.*, *30*(10), 1500, doi:10.1029/2003GL017017.

Thompson, A. M., J. C. Witte, R. D. Hudson, H. Guo, J. R. Herman, and M. Fujiwara (2001), Tropical tropospheric ozone and biomass burning, *Science*, *291*, 2128–2132.

Weber, R. J., D. Orsini, Y. Daun, Y.-N. Lee, P. J. Klotz, and F. Brechtel (2001), A particle-into-liquid collector for rapid measurement of aerosol bulk chemical composition, *J. Aerosol Sci. Technol.*, *35*, 718–727.

Wotawa, G., and M. Trainer (2000), The influence of Canadian forest fires on pollutant concentrations in the United States, *Science*, *288*, 324–328.

Yokelson, R. J., I. T. Bertschi, T. J. Christian, P. V. Hobbs, D. E. Ward, and W. M. Hao (2003), Trace gas measurements in nascent, aged, and cloud-processed smoke from African savanna fires by airborne Fourier transform infrared spectroscopy (AFTIR), *J. Geophys. Res.*, *108*(D13), 8478, doi:10.1029/2002JD002322.

Zondlo, M. A., R. L. Mauldin, E. Kosciuch, C. A. Cantrell, and F. L. Eisele (2003), Development and characterization of an airborne-based instrument used to measure nitric acid during the NASA Transport and Chemical Evolution Over the Pacific field experiment, *J. Geophys. Res.*, *108*(D20), 8793, doi:10.1029/2002JD003234.

M. A. Avery, E. V. Browell, G. Chen, J. Crawford, G. W. Sachse, and S. A. Vay, NASA Langley Research Center, Hampton, VA 23681, USA. (m.a.avery@larc.nasa.gov; edward.v.browell@nasa.gov; g.chen@larc.nasa.gov; j.h.crawford@larc.nasa.gov; g.w.sachse@larc.nasa.gov; s.a.vay@larc.nasa.gov)

D. R. Blake, Department of Chemistry, University of California, Irvine, CA 92697-2025, USA. (drblake@uci.edu)

A. D. Clarke, School of Ocean and Earth Science and Technology, University of Hawaii at Manoa, Honolulu, HI 96822, USA. (tclarke@soest.hawaii.edu)

F. L. Eisele, F. Flocke, and A. J. Weinheimer, Atmospheric Chemistry Division, National Center for Atmospheric Research, Boulder, CO 80303, USA. (eisele@ucar.edu; ffl@acd.ucar.edu; wein@ucar.edu)

H. E. Fuelberg, Department of Meteorology, Florida State University, Tallahassee, FL 32306, USA. (fuelberg@met.fsu.edu)

K. Kita, Department of Environmental Science, Ibaraki University, Bunkyo 2-1-1, Mito, 310-8512 Ibaraki, Japan. (kita@env.sci.ibaraki.ac.jp)

M. Koike, Earth and Planetary Science, Graduate School of Science, University of Tokyo, 7-3-1 Hongo, Bunkyo-ku, 113-0033 Tokyo, Japan. (koike@eps.s.u-tokyo.ac.jp)

Y. Kondo, Y. Miyazaki, Y. Morino, and N. Takegawa, Research Center for Advanced Science and Technology, University of Tokyo, 4-6-1 Komaba, Meguro-ku, 153-8904 Tokyo, Japan. (kondo@atmos.rcast.u-tokyo.ac.jp; yuzom@atmos.rcast.u-tokyo.ac.jp; morino@atmos.rcast.u-tokyo.ac.jp; takegawa@atmos.rcast.u-tokyo.ac.jp)

B. Liley, National Institute of Water and Atmospheric Research, Lauder, New Zealand. (b.liley@niwa.co.nz)

S. T. Sandholm and R. J. Weber, Department of Earth and Atmospheric Sciences, Georgia Institute of Technology, Atlanta, GA 30332, USA. (scott.sandholm@eas.gatech.edu; rweber@eas.gatech.edu)

H. B. Singh, NASA Ames Research Center, Moffet Field, CA 94035, USA. (hsingh@mail.arc.nasa.gov)

D. G. Streets, Argonne National Laboratory, Argonne, IL 60439, USA. (dstreets@anl.gov)

R. W. Talbot, Institute for the Study of Earth, Oceans, and Space, University of New Hampshire, Durham, NH 03820, USA. (robert.talbot@unh.edu)

M. A. Zondlo, Southwest Sciences, Inc., 1570 Pacheco St., Suite E-11, Santa Fe, NM 87505, USA. (mzondlo@swsciences.com)